Tropical Cyclone Diurnal Cycle Signals in a Hurricane Nature Run

JASON P. DUNION

Cooperative Institute for Marine and Atmospheric Studies, University of Miami, and NOAA/Atlantic Oceanographic and Meteorological Laboratory/Hurricane Research Division, Miami, Florida

CHRISTOPHER D. THORNCROFT

University at Albany, State University of New York, Albany, New York

DAVID S. NOLAN

Rosenstiel School of Marine and Atmospheric Science, University of Miami, Miami, Florida

(Manuscript received 13 April 2018, in final form 19 November 2018)

ABSTRACT

The diurnal cycle of tropical convection and tropical cyclones (TCs) has been previously described in observational-, satellite-, and modeling-based studies. The main objective of this work is to expand on these earlier studies by identifying signals of the TC diurnal cycle (TCDC) in a hurricane nature run, characterize their evolution in time and space, and better understand the processes that cause them. Based on previous studies that identified optimal conditions for the TCDC, a select period of the hurricane nature run is examined when the simulated storm was intense, in a low shear environment, and sufficiently far from land. When analyses are constrained by these conditions, marked radially propagating diurnal signals in radiation, thermodynamics, winds, and precipitation that affect a deep layer of the troposphere become evident in the model. These propagating diurnal signals, or TC diurnal pulses, are a distinguishing characteristic of the TCDC and manifest as a surge in upper-level outflow with underlying radially propagating tropical squall-line-like features. The results of this work support previous studies that examined the TCDC using satellite data and have implications for numerical modeling of TCs and furthering our understanding of how the TCDC forms, evolves, and possibly impacts TC structure and intensity.

1. Introduction

Previous studies have documented diurnal variability of tropical oceanic convection (e.g., Gray and Jacobson 1977; Mapes and Houze 1993; Liu and Moncrieff 1998; Yang and Slingo 2001) and the tropical cyclone (TC) upper-level cirrus canopy (e.g., Weickmann et al. 1977; Browner et al. 1977; Muramatsu 1983; Kossin 2002). Randall et al. (1991) and Xu and Randall (1995) found that direct radiation–convective interactions (e.g., radiative cloud-top nocturnal radiative cooling and daytime warming) were important for promoting diurnal and semidiurnal variations of precipitation over the ocean. Gray and Jacobson (1977) found that more organized weather systems are associated with more pronounced diurnal cycles of oceanic precipitation with a maximum in the morning. They hypothesized that day versus night variations in tropospheric radiational cooling between areas of convection and the surrounding cloud-free atmosphere was important for forcing the diurnal cycle of deep convection. Dunion et al. (2014) examined a phenomenon described as the TC diurnal cycle (TCDC) and found cyclical pulses in the cloud field (as seen by infrared satellite imagery) that propagate radially outward from mature TCs at speeds of 5–10 m s^{-1} and through a deep layer of the troposphere. These diurnal pulses, a distinguishing characteristic of the TCDC (and possibly other forms of organized tropical convection), begin forming in the storm's inner core near the time of sunset each day and appear as a region of cooling cloud-top temperatures. The area of cooling subsequently takes on a ringlike appearance as marked cloud-top warming begins to occur on its inside edge and it begins to move away from the storm overnight, reaching several

Corresponding author: Jason P. Dunion, jason.dunion@noaa.gov

DOI: 10.1175/MWR-D-18-0130.1

hundred kilometers from the circulation center by the following afternoon. Dunion et al. (2014) also presented a 24-h conceptual clock that describes the TCDC evolution and predicts the approximate arrival time (LST) of TC diurnal pulses at various radii from the storm center each day. This conceptual clock has utility for identifying the position and evolution of TC diurnal pulses in observational datasets and numerical simulations. Although Dunion et al. (2014) proposed several hypotheses regarding the mechanisms driving the TCDC and TC diurnal pulses, the exact nature of this potentially fundamental TC process remains unclear.

A study by Bu et al. (2014) used a preimplementation of the 2013 operational HWRF Model to examine aspects of cloud radiative forcing (CRF) and how the interaction of hydrometeors with atmospheric radiation can influence the structure and intensity of TCs. Compared to runs with CRF turned off, CRF-active simulations permitted hydrometeors to more consistently modulate longwave and shortwave radiative tendencies, especially in the TC cirrus outflow layer, and produced storms with more convection and diabatic heating outside the eyewall, a wider eye, a broader wind field, and a stronger secondary circulation. Tang and Zhang (2016) used the Advanced Research version of the WRF Model (WRF-ARW) to examine the impacts of the diurnally varying radiation cycle on the formation, intensity, structure, and track of 2014 Hurricane Edouard. They found that in the absence of nighttime conditions (i.e., daytime only with the solar insolation continuously set at local noon), a simulated TC failed to develop because of a lack of nighttime cooling and destabilization that typically enhances the primary storm vortex. They also concluded that nighttime destabilization was a key factor in stimulating convection outside the TC inner core, eventually promoting the development of outer rainbands and increasing the size of the storm.

Navarro and Hakim (2016) used an axisymmetric, nonhydrostatic cloud model to examine the role of the diurnal cycle of radiation on axisymmetric hurricane structure. They found coherent diurnal signals in temperature, wind, and latent heating tendency fields that account for up to 62% of the variance in the TC outflow layer and 28% of the variance in the TC boundary layer. They hypothesized that the TCDC is a combined response from two distinct circulations in the storm: a radiatively driven circulation in the outflow layer due to absorption of solar radiation and a convectively driven circulation in the lower and middle troposphere due to anomalous latent heating that is linked to a diurnal cycle of anomalous convection. O'Neill et al. (2017) also examined diurnal responses in simulated TCs. They found that internal inertial gravity waves (i.e., diurnal waves) are favored to form outside the TC inner core and that the anticyclonic outflow region of the storm is most receptive to these radially propagating features.

The main goal of the current study is to examine a highly realistic simulation of an Atlantic hurricane to identify signals of the TCDC in the model, characterize these signals in time and space, and better understand the processes that cause them. For this purpose, we employ the "hurricane nature run" previously described and validated by Nolan et al. (2013, hereafter N13). Using criteria described by Dunion et al. (2014), a select period of the nature run is examined when the simulated hurricane was intense, in a low vertical wind shear environment, and sufficiently far from land. When analyses are constrained by these conditions, marked diurnal signals in radiation, thermodynamics, static stability, winds, and precipitation become evident in the simulation. This study begins with a focus on radiation in the hurricane nature run environment and includes analyses of OLR, as well as temperature tendencies caused by shortwave, longwave, and total radiation. Discussion will then shift to include analyses of thermodynamics, static stability, winds, and finally precipitation. There are two aspects of the TCDC that are addressed by these discussions: 1) detection of the TCDC and radially propagating TC diurnal pulses and 2) diurnal priming of the TC environment that promotes the occurrence of convectively active, radially propagating TC diurnal pulses. The findings confirm the satellite-based TCDC findings discussed by Dunion et al. (2014) and have implications for numerical modeling of TCs and furthering our understanding of how the TCDC forms, evolves, and possibly impacts TC structure and intensity.

2. Data

The high-resolution, full-physics simulation of a hurricane used for this study is the first hurricane nature run (HNR1) described by N13. HNR1 is a 13-day regionally downscaled simulation of a hurricane that occurs in the 13-month joint OSSE nature run that was produced by the European Centre for Medium-Range Weather Forecasts (Andersson and Masutani 2010). The validation, strengths, and weaknesses of the hurricane evolution and structure in HNR1 were discussed thoroughly in N13. HNR1 has been used in several hurricane OSSE studies (e.g., Atlas et al. 2015; McNoldy et al. 2017) as well as to investigate physical processes such as rapid intensification (Miyamoto and Takemi 2015) and secondary eyewall formation (Kepert and Nolan 2014).

HNR1 uses a large outer domain that covers the tropical Atlantic and three nested grids that move with the simulated cyclone. All data for this study are taken

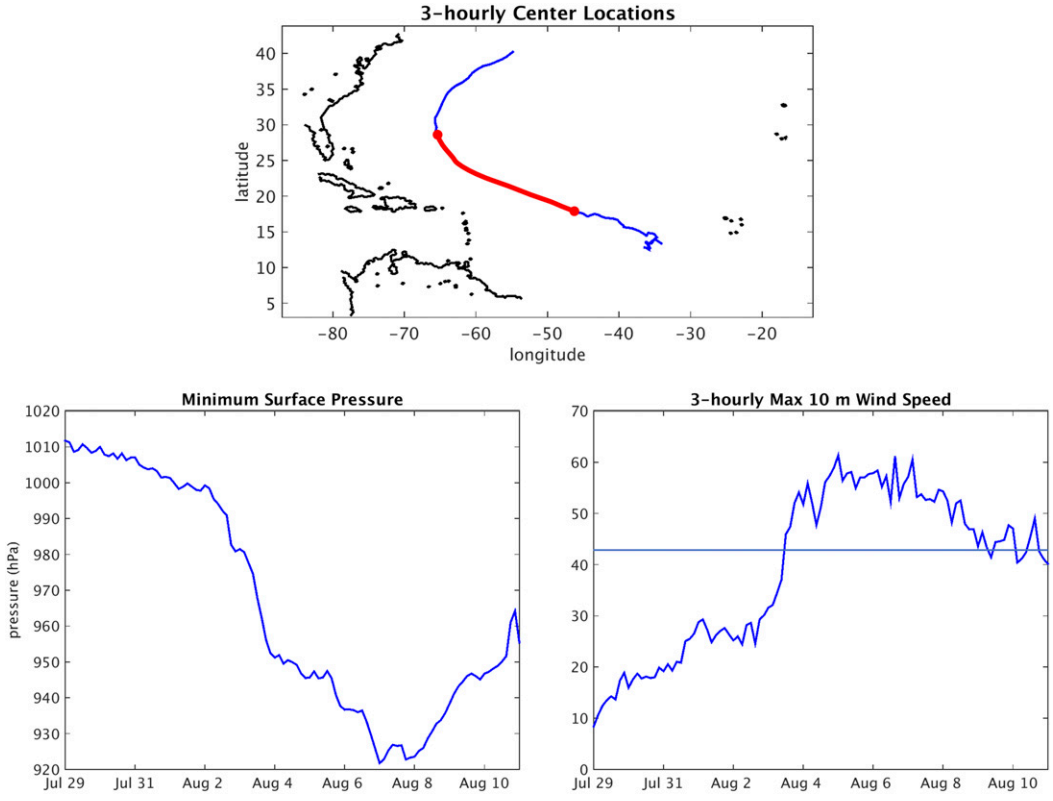

FIG. 1. The 3-hourly (top) track, (bottom left) minimum surface pressure, and (bottom right) maximum 10-m wind speed for the 13-day HNR1 simulation. The red curve on the track plot shows the 3–8 Aug HNR1 study period and the light blue line in the 10-m wind speed plot denotes the Saffir–Simpson hurricane wind scale category 2 wind speed threshold (43 m s^{-1}).

from the first nested grid that has 120 × 120 grid points with 9-km grid spacing. While the inner grids have higher resolution, their sizes are smaller than the typical propagation distance of the TC diurnal pulse that can extend at least 300 km from the center. The 9-km grid allows the analysis to extend out to 540 km. The storm track, peak wind speed, and minimum surface pressure computed from the 9-km grid are shown in Fig. 1. Additional details of the HNR1 configuration are shown in Table 1.

The HNR1 TC exhibited a life cycle typical of a North Atlantic Cape Verde–type system (Dunn and Miller 1960), as it formed from an African easterly wave, intensified into a Saffir–Simpson (SS) hurricane wind scale category 4 hurricane (≥58 m s^{-1}), and eventually recurved after reaching ~65°W. The life cycle of this sequence spans a 13-day period from 0000 UTC 29 July to 0000 UTC 11 August 2005. Dunion et al. (2014) found that the TCDC was most pronounced in mature hurricanes [SS intensity of category 2 or higher (≥43 m s^{-1})] that were in relatively low shear environments (≤7.5 m s^{-1} of 200–850-hPa vertical wind shear; Gallina and Velden 2000; Dunion 2011) and located ≥300 km from land, and constrained their storm sample composite accordingly. This study uses these same thresholds to identify the portion of the HNR1 TC life cycle that would be most conducive for TCDC processes. Figure 1 indicates that the storm met the minimum distance to land threshold for the entire period and that the intensity requirement was attained from days 5 to 10. Finally, N13 showed that the vertical wind shear affecting the HNR1 TC during this 5-day period never exceeded 7.5 m s^{-1} (see Fig. 8 of N13). Therefore, days 5–10 (0000 UTC 3 August–0000 UTC 8 August) of the HNR1 simulation were examined for signs of the TCDC.

3. Results

a. Radiation

1) Outgoing longwave radiation (OLR)

OLR represents the total longwave infrared energy radiating from Earth to space and is affected by surface temperature and emissivity, atmospheric temperature,

TABLE 1. HNR1 model, domain, resolution, and physics.

Model configuration	
Model	Weather Research and Forecasting (WRF) Model v3.2.1
Horizontal resolution	4 nested domains: 27-, 9-, 3-, and 1-km grid spacing (data from the 9-km grid used in this study)
Vertical resolution	61 full model levels (up to 50 hPa)
Atmospheric processes	
Microphysics	WRF single-moment 6-class microphysics scheme (WDM6)
Radiation	RRTMG schemes for both shortwave and longwave radiation (called every 6 min)
Convection	Kain–Fritsch convective parameterization (active on domain 1 and domain 2)
Boundary layer surface fluxes and turbulent mixing	Yonsei University (YSU) planetary boundary layer scheme [surface drag coefficient modeled after Donelan et al. (2004)]
Oceanic processes	
Mixed layer	Pollard et al. (1972) one-dimensional model as implemented in WRF 3.2.1
Mixed layer depth	25 m
Thermocline stratification	0.1 m^{-1} (top of thermocline)

water vapor profile, and cloud cover. It is expected that OLR should correlate highly with the findings of Dunion et al. (2014) that used the 10.7- and 10.8-μm channels on the GOES and Meteosat satellites to detect the TCDC and associated TC diurnal pulses propagating away from the storm. Figure 2 shows a Hovmöller diagram of OLR for the first 10 days of the life cycle of the HNR1 TC before it began to recurve into the midlatitudes and weaken below category-2 intensity. This figure reveals a marked diurnal oscillation in the OLR pattern that becomes established over a radius (R) range of ~150–450 km beginning on day 5 (3 August) and continues through day 10 (8 August), the only period in the HNR1 when all three TCDC criteria are satisfied. This figure also suggests that the OLR signal appears to propagate away from the storm each day. Diurnal fluctuations of $\pm$20–60 W m^{-2} are evident at R = 150–250 km, while larger fluctuations of $\pm$45–70 W m^{-2} occur at R = 350–450 km. These fluctuations indicate that a distinct radially propagating OLR diurnal cycle signal is evident in the HNR1 TC with R = 150–450 km OLR maxima from ~0000–0600 UTC (~2000–0200 LST) and OLR minima from ~1400–2000 UTC (~1000–1600 LST) each day. The diurnal timing of these longwave infrared peaks and troughs are similar to those described in previous studies (e.g., Kossin 2002; Dunion et al. 2014) and the ~10 m s^{-1} radial propagation speed indicated in Fig. 2 is also similar to the TCDC described by Dunion et al. (2014). Given the location of the HNR1 TC over the ocean throughout the simulation, this diurnal infrared radiation signal is likely arising through a combination of variations in atmospheric cloud-top height and depth, as well as atmospheric temperature and moisture. Several of the sections that follow include detailed analyses of these various contributions to the OLR.

2) SHORTWAVE, LONGWAVE, AND TOTAL RADIATION

Since the TCDC has been linked to the solar cycle (Dunion et al. 2014), analyses were made of shortwave, longwave, and total radiation temperature tendency for the HNR1 domain from 3 to 8 August at 200, 700,

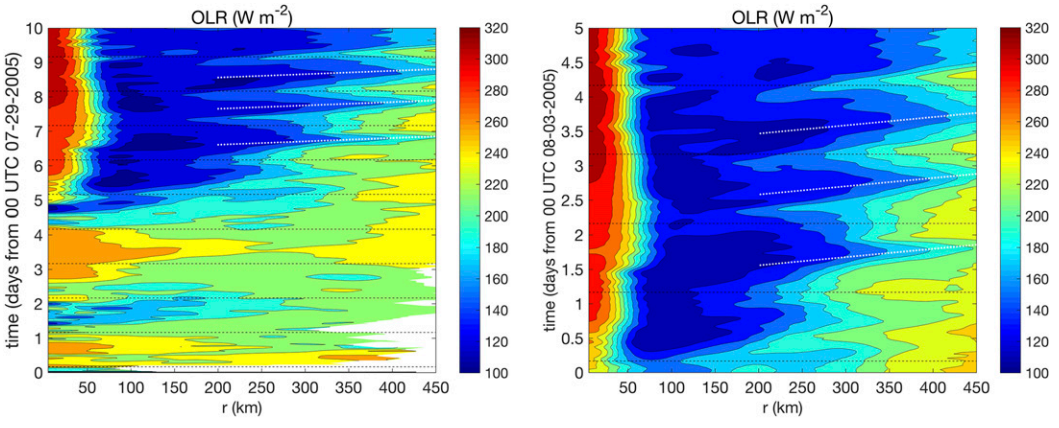

FIG. 2. Hovmöller diagrams of azimuthally averaged OLR (W m^{-2}) calculated for (left) the period from 29 Jul to 8 Aug of the HNR1 and (right) only for the 3–8 Aug HNR1 study period. Dashed black lines denote 0000 LST during each day of the simulation. Dashed white lines indicate radial propagation (~10 m s^{-1}) of the OLR signal from 4 to 6 Aug. Radii are analyzed relative to the TC center and extend out to 450 km.

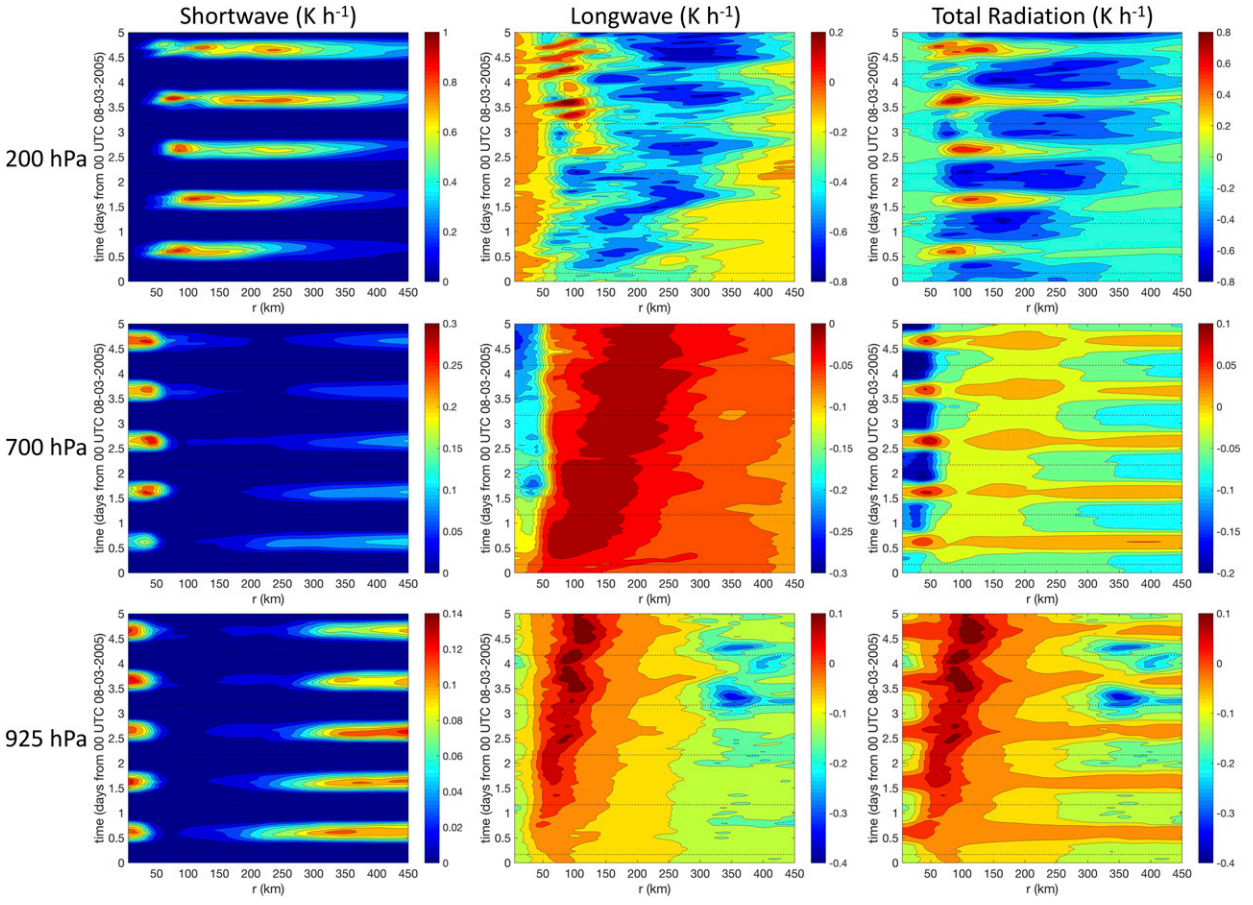

FIG. 3. Hovmöller diagrams of azimuthally averaged shortwave, longwave, and total radiation tendencies (K h^{-1}) derived from the HNR1. Analyses are derived over the 3–8 Aug study period and show the 200-, 700-, and 925-hPa pressure levels. Dashed black lines denote 0000 LST during each day of the simulation. Radii are analyzed relative to the TC center and extend out to 450 km.

and 925 hPa (Fig. 3). Not surprisingly, shortwave tendencies show regular oscillations of net warming that are associated with the daily solar cycle and influenced by the three-dimensional distribution of clouds in the storm. Near the outflow layer (~200 hPa), maximum daytime warming takes place from $R \sim 50$–300 km due to the presence of cirrus clouds in that region of the storm (Fig. 4). There is little warming inside of $R \sim 50$ km due to the relatively cirrus-free eye region of the storm and a general trend for reduced peak warming with increasing radii beyond $R \sim 350$–300 km, which is due to the presence of generally less optically thick clouds with increasing radius from the storm, as suggested by Fig. 4. Although daytime shortwave warming (~0.3–1.0 K h^{-1}) occurs in the upper levels of the TC (e.g., 200 hPa) from $R \sim 25$–450 km, lower to midlevels (e.g., 700 and 925 hPa) experience near-zero shortwave warming during the day from just outside the eye to $R \sim 150$–250 km where the ice mixing ratio at high altitude suggests the presence of a diurnally varying cirrus outflow layer that is optically thicker each afternoon (Figs. 2 and 4) that would act to block incoming shortwave radiation (Figs. 4 and 5).

Longwave infrared tendencies generally produce a net cooling in the upper levels across the HNR1 domain, although there are preferred times of day when the cooling rate appears to be more pronounced. At 200 hPa, peak longwave cooling occurs in the daytime, reaches a minimum at night, and is positively correlated with the diurnal cycle of ice mixing ratio (Fig. 5). Although the cloud-free atmosphere is relatively transparent to longwave IR radiation emitted from Earth, the TC cirrus outflow layer becomes increasingly efficient at absorbing this longwave radiation as these daytime radial surges of high cirrus occur and the layer becomes optically thicker in the HNR1 simulation. The longwave IR energy that is absorbed by the cirrus outflow layer is reemitted both back to Earth and to the top of the atmosphere and because these cirrus clouds are high [e.g., ~7.5–14 km (~400–150 hPa); Fig. 4] and cold, the

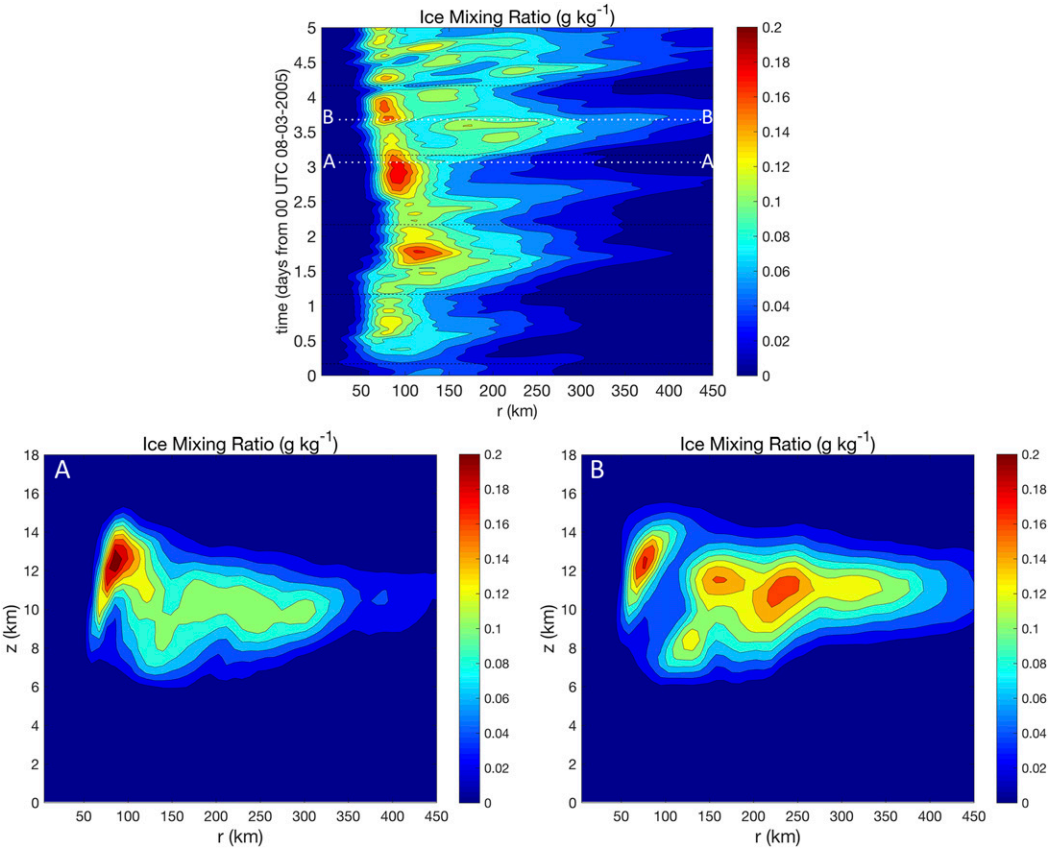

FIG. 4. (top) Hovmöller diagram of azimuthally averaged ice mixing ratio (g kg^{-1}) derived from the 3–8 Aug HNR1 study period for 200 hPa. Dashed black lines denote 0000 LST during each day of the simulation. Radius–height cross sections of azimuthally averaged ice mixing ratio derived from the HNR1 at (a) 0100 UTC (2100 LST) 6 Aug and (b) 1600 UTC (1200 LST) 6 Aug are also shown. The white dashed lines in the Hovmöller diagram show times from which the cross sections were derived. Radii in all plots are analyzed relative to the TC center and extend out to 450 km.

longwave energy radiated to the top of the atmosphere is less than it would be in the absence of cloud or in an optically thinner layer of cloud. Figure 4 indicates that in the late morning/early afternoon, the radial extent of the TC cirrus canopy is greater and contains ice mixing ratio values from $z \sim 6$–15 km that are a factor of 2–10 times higher than they are in the evening. The higher, optically thicker surges of cirrus clouds from the late morning to early afternoon could explain the daytime peak in longwave cooling seen in the upper levels each day (Figs. 4 and 5).

The radius–height cross sections of azimuthally averaged shortwave, longwave, and total radiation tendency in Figs. 6–8 show the three-dimensional radiation profiles of the HNR1 TC from 6 to 7 August and illustrate radiative processes of the background TC environment that may be priming the environment to support the TCDC. These figures include two elevated regions, A and B, that both extend from 3 to 13 km in the vertical and span from $R = 50$–200 km to $R = 200$–400 km in the horizontal, respectively. These horizontal and vertical ranges were chosen to capture an area of persistent net warming that occurs throughout the day from $R \sim 50$–450 km (Fig. 8) that could have important implications for local static stability and to highlight the area of the TC inner core ($R \leq 150$–200 km; Rogers et al. 2012) versus the surrounding environment ($R \geq 150$–200 km). While the outer edge of region A corresponds to the approximate radius range of TC diurnal pulse initiation that was noted by Dunion et al. (2014), regions A and B both experience patterns of net radiation tendencies that may be important for TCDC processes. For Figs. 6–8, nighttime is ~2100–0300 LST, dawn is ~0600 LST, daytime is ~0900–1500 LST, and dusk is ~1800 LST.

Figures 6 and 7 indicate that shortwave warming during the daytime and longwave cooling at night are preferentially occurring in the cirrus outflow layer (i.e., areas of enhanced ice mixing ratio, Fig. 4). Since the

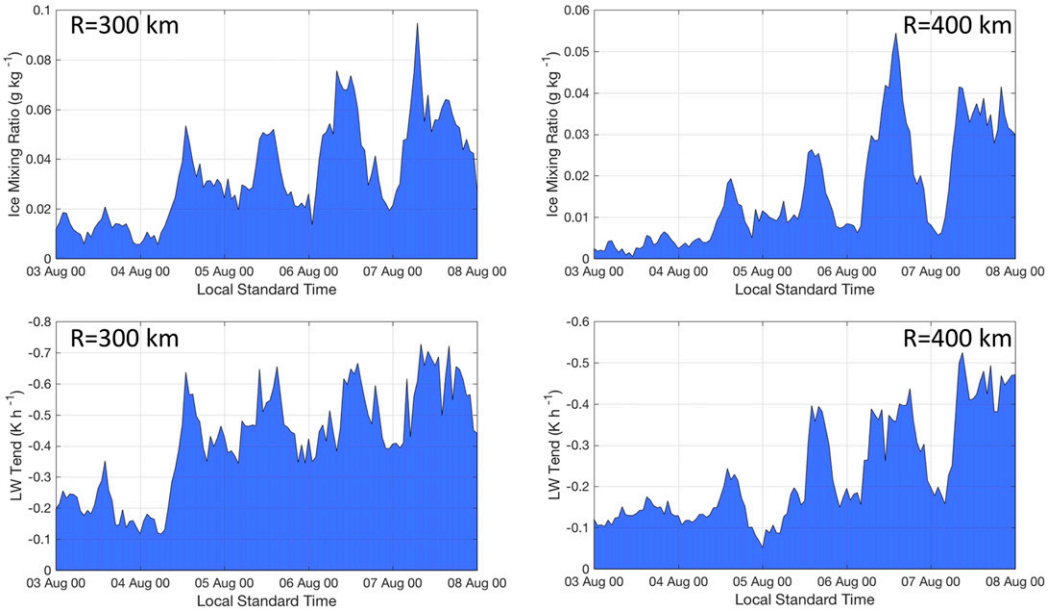

FIG. 5. 200-hPa azimuthally averaged (top) ice mixing ratio (g kg^{-1}) and (bottom) longwave radiation tendency (K h^{-1}) derived from the 3–8 Aug HNR1 study period at 300 and 400 km radii.

upper 3–5 km of the HNR1 TC outflow layer lowers with increasing radius, relatively more shortwave warming and longwave cooling occurs in the mid- to upper levels of region B compared to region A. During the day, shortwave warming is greater than opposing longwave cooling in the upper few kilometers of regions A and B ($z \sim$ 10–13 km) and could be a time when the level of neutral buoyancy (LNB) descends and convective available potential energy (CAPE) is reduced for near-surface air parcels (Fig. 8). CAPE describes the maximum buoyancy an undiluted parcel of air would have if lifted from the surface or near surface vertically through the atmosphere up to its LNB. LNB, or equilibrium level (EL) is the level at which an air parcel, rising or descending adiabatically, reaches the same temperature as its environment. During the nighttime, longwave cooling dominates the upper few kilometers of regions A and B ($z \sim$ 8–13 km) and could be a time when the LNB rises and CAPE increases. These times of warming and cooling may represent key periods that influence the daytime and nighttime evolution of the TCDC and will be discussed more in section 3b(3).

b. *Thermodynamics and stability*

1) TEMPERATURE

Analyses of potential temperature θ were conducted to search for signs of the TCDC in the HNR1 thermodynamic fields. These analyses reveal distinct diurnal signals at various atmospheric levels (e.g., 200, 700, and 925 hPa, and the near surface) and radii. At upper levels (e.g., 200 hPa), there is no robust diurnal signal in the inner 150 km of the storm. However, there is a distinct diurnal θ pattern just outside of 150 km with maxima around local noon and minima around local midnight (Fig. 9). The θ patterns in this region of the storm, corresponding to the outer edge of the TC inner core, are positively correlated with upper-level shortwave and total radiation tendencies, and are negatively correlated with longwave radiation tendencies (Fig. 3). These diurnal θ patterns also appear to be propagating radially away from the TC (Fig. 9) and are closely matched in time and space with OLR (Fig. 2) and ice mixing ratio (Fig. 4). This suggests that diurnal variability of radiation (enhanced in the presence of ice in the TC outflow layer) are driving the upper-level θ patterns at $R \sim$ 150–450 km. Values of θ at upper levels begin cooling each afternoon and reach a minimum around local midnight, which implies that this region of the storm experiences regular occurrences of destabilization via cooling of the environmental profile in the upper levels (e.g., an elevated LNB and higher CAPE) from the late afternoon into the evening, which could help promote convection locally (Fig. 9).

The midlevels (e.g., 700 hPa) of the HNR1 TC do not exhibit robust diurnal θ fluctuations in the inner 300 km of the storm (Fig. 9). There is a modest diurnal signal from $R \sim$ 300–450 km with peak warming (cooling) in the evening to local midnight (predawn hours) and θ fluctuations of ~0.5–1 K. In contrast, diurnal θ patterns

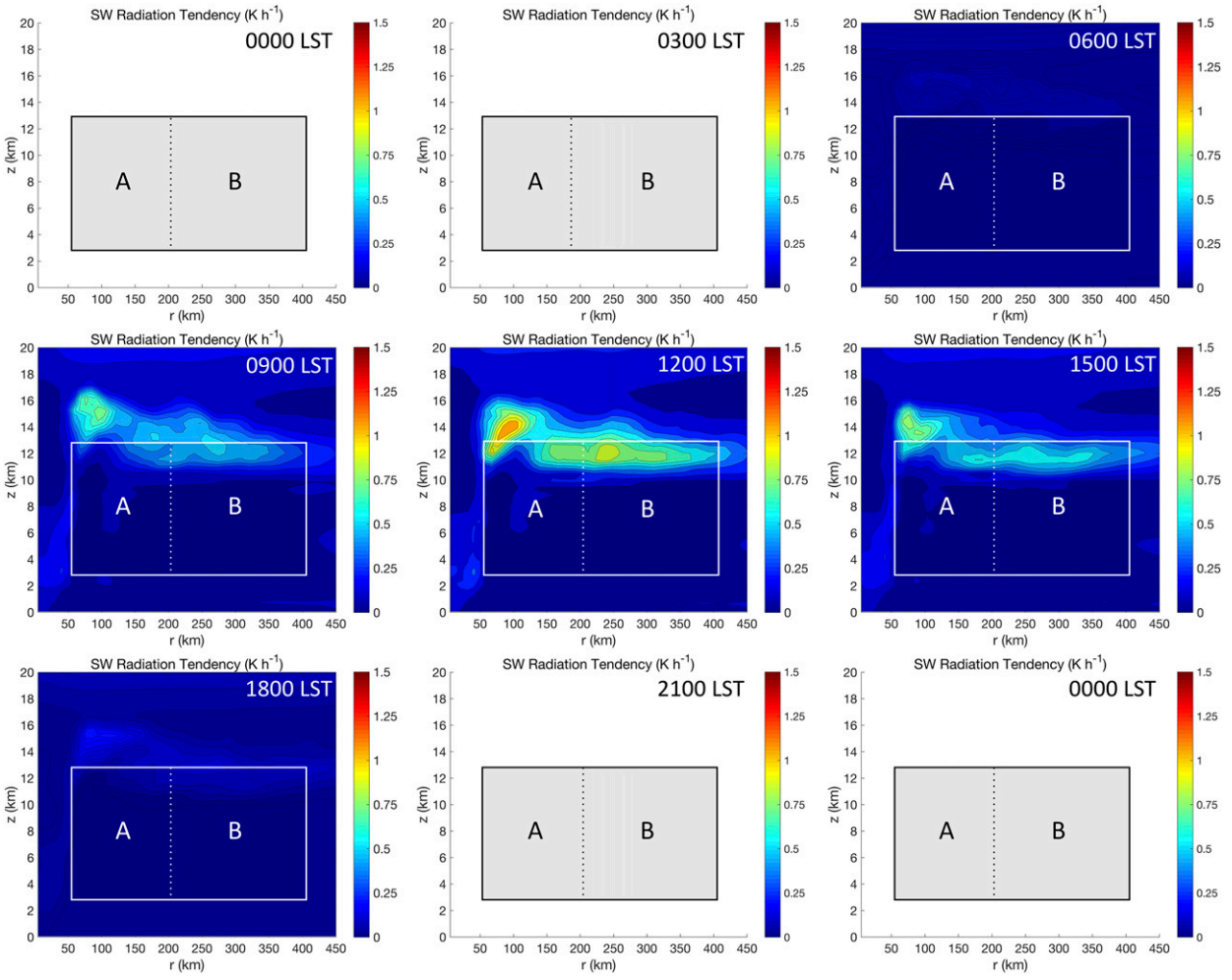

FIG. 6. 3-hourly radius–height cross sections of azimuthally averaged shortwave radiation tendency (K h^{-1}) derived from the HNR1 from 0000 LST 6 Aug to 0000 LST 7 Aug. The shaded boxes highlight the regions from z = 3–13 km from R = 50–200 km (box A) and R = 200–400 km (box B). Radii are analyzed relative to the TC center and extend out to R = 450 km.

are quite evident in the lower levels (e.g., 925 hPa and 40 m) of the HNR1 TC environment, particularly from 5 to 8 August (Fig. 9). At 925 hPa and especially 40 m, the diurnal θ signals appear to be propagating outward from the storm each afternoon. The 40-m near-surface diurnal fluctuations range from ~0.5 to 1.5 K and suggest that the TC diurnal cycle is periodically associated with cooler near-surface temperatures each day. It should be noted that the HNR1 uses a 1D mixed layer model that cools the upper ocean due to shear-induced mixing with water in the thermocline. It also accounts for solar and longwave radiation, with the net result being a weak diurnal cycle in SST of about ±0.1 K day^{-1}.

2) MOISTURE

The HNR1 TC exhibits distinct diurnal signals in water vapor mixing ratio at all levels (Figs. 10 and 11). At upper levels (e.g., 200 hPa), these oscillations are most pronounced from R = 150–450 km, peak around local noon at inner radii, and appear to propagate away from the storm during the afternoon. Variations in 200-hPa mixing ratio have a distinct diurnal pattern that is similar to previously shown patterns of OLR and potential temperature, suggesting that the TCDC signal is characterized by marked changes in both temperature and moisture.

At midlevels of the HNR1 TC (e.g., 700 hPa), there is a less well-defined diurnal pattern of mixing ratio throughout the domain (Fig. 10). However, at R = 150–300 km, there are prominent radially propagating diurnal peaks in midlevel mixing ratio that occur in the late evening through early morning hours each day (Figs. 10 and 11). These maxima are regularly interspersed by ebbs in mixing ratio that occur in the

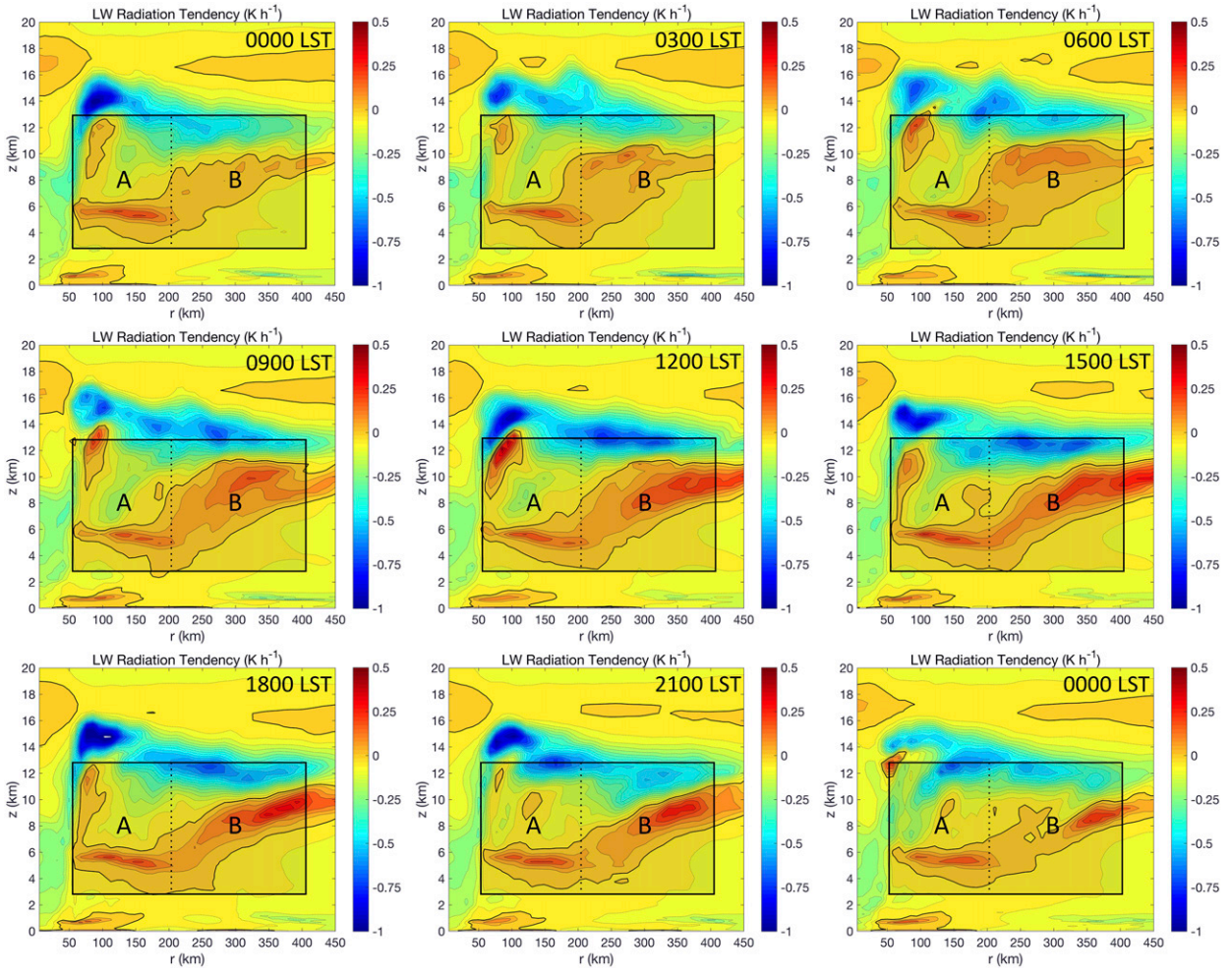

FIG. 7. 3-hourly radius–height cross sections of azimuthally averaged longwave radiation tendency (K h^{-1}) derived from the HNR1 from 0000 LST 6 Aug to 0000 LST 7 Aug. The shaded boxes highlight the regions from z = 3–13 km from R = 50–200 km (box A) and R = 200–400 km (box B). Bold contours denote regions of zero net radiation tendencies. Radii are analyzed relative to the TC center and extend out to R = 450 km.

mid- to late afternoon, are 0.5–2.5 g kg^{-1} dryer, and appear to be ~12 h out of phase with the upper-level values (e.g., 200 hPa).

The lower levels (e.g., 925 hPa and 40 m) of the HNR1 TC show a robust TCDC of mixing ratio that tends to be at a minimum in the late morning to late afternoon hours and is most evident from $R \sim$ 100–300 km (Figs. 10 and 11). These minima exhibit signs of radial propagation from R = 150–350 km and are regularly interspersed by periods of significantly greater mixing ratio (~0.5–2.5 g kg^{-1}).

3) LNB AND CAPE

CAPE in this study is computed from vertical profiles, assume that a surface parcel is represented by the mean temperature and moisture in the lowest 500 m of each sounding profile that was computed across the HNR1 domain, and is based on irreversible moist-adiabatic processes. CAPE exhibits a distinct diurnal cycle that is especially pronounced from 5 to 8 August (Fig. 12). CAPE displays diurnal signals that are most pronounced from $R \sim$ 150–300 km. It tends to peak in the early morning hours between approximately local midnight and 0900 LST, with lowest values from the late morning to late afternoon. Cape values are consistently low (~0–500 J kg^{-1}) inside of $R \sim$ 150 km. Diurnal variations in radiation tendency at critical levels appear to be impacting the environmental temperature profile and hence, the LNB and CAPE. The diurnal signals of the LNB and CAPE (Fig. 12) appear to be in phase with the patterns of mid- to upper-level ($z \sim$ 4–10 km) total radiation tendencies that were previously discussed. It was

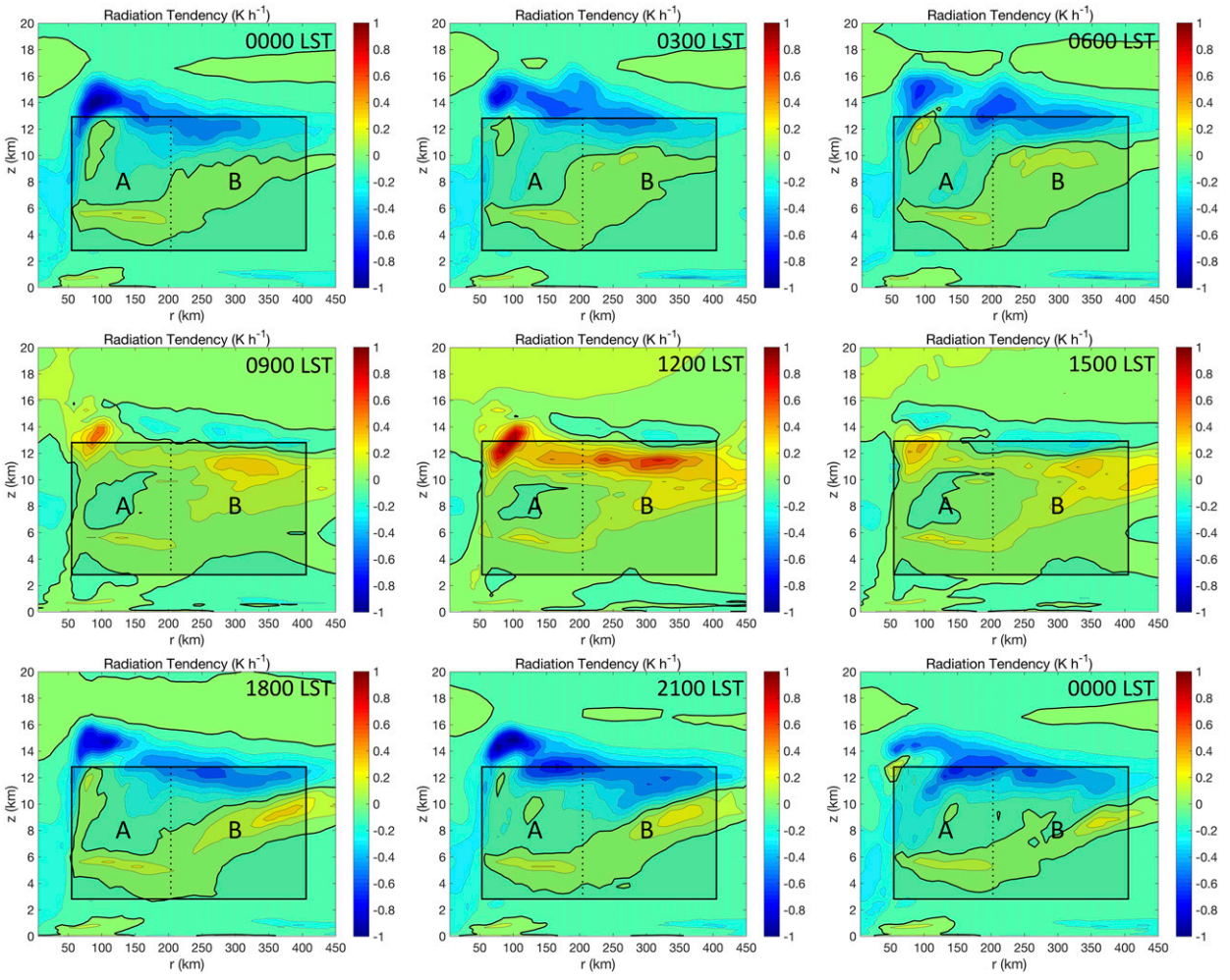

FIG. 8. 3-hourly radius–height cross sections of azimuthally averaged total radiation tendency (K h^{-1}) derived from the HNR1 from 0000 LST 6 Aug to 0000 LST 7 Aug. The shaded boxes highlight the regions from z = 3–13 km from R = 50–200 km (box A) and R = 200–400 km (box B). The bold contours denote regions of zero net radiation tendencies. Radii are analyzed relative to the TC center and extend out to R = 450 km.

hypothesized in section 3a(2) that differing radiation tendencies at various radii from R = 50–400 km may modify both the LNB and hence CAPE in the HNR1 TC environment. Throughout the study period, the radius range of $R \sim$ 50–100 km has little to no CAPE (0–500 J kg^{-1}) and LNBs as low as 600–800 hPa, which may be related to the presence of the storm's warm core, which exists in balance with the baroclinic wind field and to persistent warming that occurs in the layer from $z \sim$ 4–6 km during both the daytime and nighttime (Fig. 8). The magnitude of this warming does fluctuate diurnally and appears to be contributing to the diurnal variability of CAPE and the LNB (Fig. 12). At radii of ~150–350 km, CAPE and the LNB fluctuate diurnally by as much as 1500 J kg^{-1} and 450 hPa, respectively, and are remarkably in phase throughout the day. As the LNB pressure level increases (decreases), corresponding CAPE values decrease (increase). It is also evident that at R = 150–200 km, there is a general linear decrease (lowering) of CAPE (the LNB) as the simulation progresses, which may be linked to radial expansion of the HNR1 TC warm core and the upper-level outflow layer (Figs. 2–5). Over time, priming of the atmosphere becomes somewhat less favored at these radii, especially at R = 150 km.

Figure 13 shows the 3-hourly progression of CAPE in the HNR1 TC inner core and surrounding environment from 0200 LST 6 August to 0200 LST 7 August. In the early morning of 6 August (0200–0500 LST), a fairly symmetric region of very low CAPE (~0–500 J kg^{-1}) exists in the inner ~150–200 km of the storm and is immediately surrounded by areas of higher CAPE (~1500–3000 J kg^{-1}) that extend out to the edges of the 9-km domain. This circle

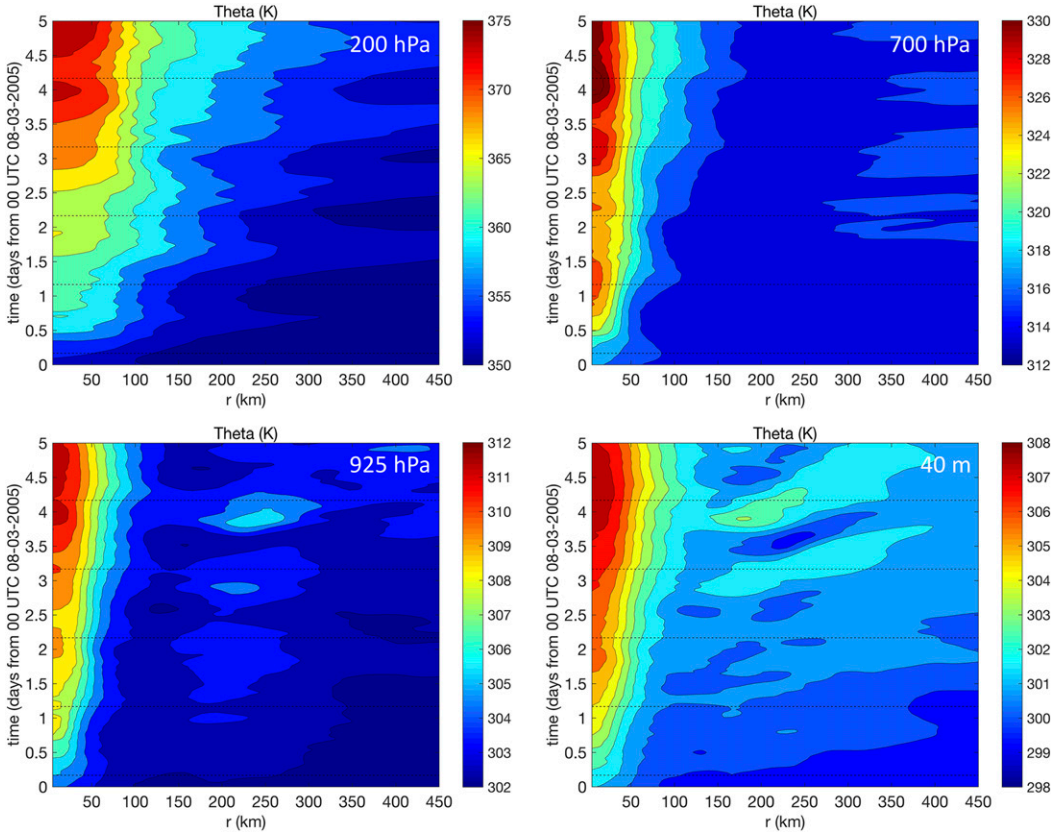

FIG. 9. Hovmöller diagrams of azimuthally averaged potential temperature (K) derived from the 3–8 Aug HNR1 study period for 200 hPa, 700 hPa, 925 hPa, and 40 m. Dashed black lines denote 0000 LST during each day of the simulation. Radii are analyzed relative to the TC center and extend out to 450 km.

of inner-core low CAPE begins to radially expand near the time of sunrise (~0530 LST) and continues to grow through the early to late afternoon, eventually reaching $R \sim 300$–400 km. The expanding area of low CAPE during the daytime also concurs with the Fig. 8 depiction of marked daytime radiational warming in the mid- to upper levels ($z \sim 6$–12 km) and corresponding 0.5–3.5-K diurnal fluctuations in θ (Fig. 9). Periods of daytime warming would act to lower the LNB, reducing the total integrated area being used to calculate CAPE, hence, reducing local values of CAPE. Starting in the early evening near the time of local sunset (i.e., ~2000 LST), the low CAPE annulus begins to dissipate along its periphery and continues to wane into the late evening until around local midnight. By the early morning hours the next day (0200 LST 7 August), the shrinking annulus of low CAPE appears to stabilize and once again extends to a radius of only ~150–200 km. Near and just outside this radius range, CAPE values increase from ~0–500 J kg^{-1} to as high as 2500 J kg^{-1} in just a few hours leading up to 0200 LST. This period of enhanced CAPE after sunset in the 150–200-km radius range could be related to the mid- to upper-level cooling noted in the corresponding areas of both regions A and B in Fig. 8. The 0–0.5 K h^{-1} cooling rates that were noted in this area just outside the inner core of the TC would promote reduced lapse rates, elevate the LNB, and increase CAPE locally. The sequence of an expanding and contracting annulus of low CAPE was also evident on days prior to and after 6–7 August (not shown).

It is hypothesized that radiational warming and cooling associated with the TC cirrus canopy and radially sloping TC anvil are producing striking fluctuations in the LNB just outside the TC inner core ($R = 150$–300 km) each day. These diurnal fluctuations in the LNB and CAPE just outside the TC inner core may also help precondition the TC environment to support convectively active TC diurnal pulses in the region of the storm just outside the inner core (i.e., $R \sim 150$–300 km).

c. *Wind*

1) SURFACE (10 M) WIND

Analyses of 10-m surface winds are presented to assess the relevance of the TCDC to forecasts of TC

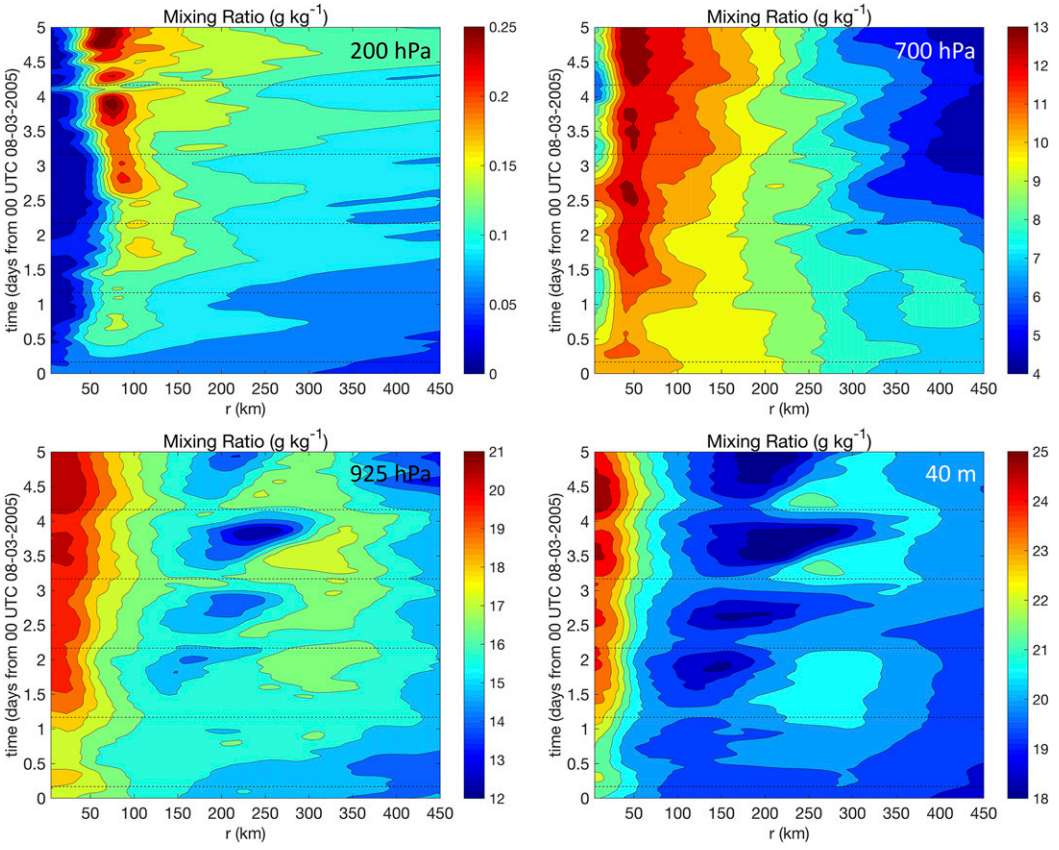

FIG. 10. Hovmöller diagrams of azimuthally averaged mixing ratio (g kg^{-1}) derived from the 3–8 Aug HNR1 study period for 200 hPa, 700 hPa, 925 hPa, and 40 m. Dashed black lines denote 0000 LST during each day of the simulation. Radii are analyzed relative to the TC center and extend out to 450 km.

intensity and structure. Surface winds show a clear diurnal signal at radii ≥50 km (Fig. 14). From R = 50–200 km, surface winds tend to peak from the late evening to early morning hours and ebb from the afternoon to late evening. These wind speed oscillations range from ~0.5–2.5 m s^{-1} and tend to be stronger with increasing radii. Although the radial and tangential components of the surface wind both exhibit diurnal fluctuations, radial wind has particularly pronounced signals (Fig. 14), such that the diurnal fluctuations of surface wind speed are largely attributable to ebbs and flows in radial winds at the surface. These diurnal fluctuations appear to be most pronounced at R ~ 150–350 km where diurnal oscillations in the magnitude of radial inflow are as strong as 4–6 m s^{-1}. The tendency for surface wind diurnal oscillations to be more pronounced at larger radii has implications for TC structure (e.g., significant wind radii). This is particularly so for the radii of 34 kt (17.5 m s^{-1}) and 50 kt (25.5 m s^{-1}) winds, which average ~230 and ~120 km, respectively, for North Atlantic major hurricanes (Demuth et al. 2006).

Analyses of 10-m surface winds show a strong diurnal signal with periods of stronger winds and more vigorous low-level inflow in the early morning hours that are interspersed with periods of weaker winds and reduced lower-level inflow from the midmorning to early afternoon. These trends in surface wind indicate a correlation between the TCDC and TC intensity and structure.

2) RADIAL WIND (NEAR SURFACE TO UPPER LEVEL)

Radial wind (V_r) tendencies in the HNR1 TC exhibit distinct diurnal patterns throughout the troposphere (Fig. 15). In the upper troposphere (e.g., 200 hPa), there appear to be daily bursts of outflow outside of ~100–150 km that develop in the early morning hours each day and steadily propagate away from the storm at speeds (5–10 m s^{-1}) similar to those described in previous studies (e.g., Navarro and Hakim 2016; Dunion et al. 2014; Ruppert and Hohenegger 2018), reaching R = 450 km in the afternoon. These daily maxima in outflow steadily strengthen through the study period, are strongest from

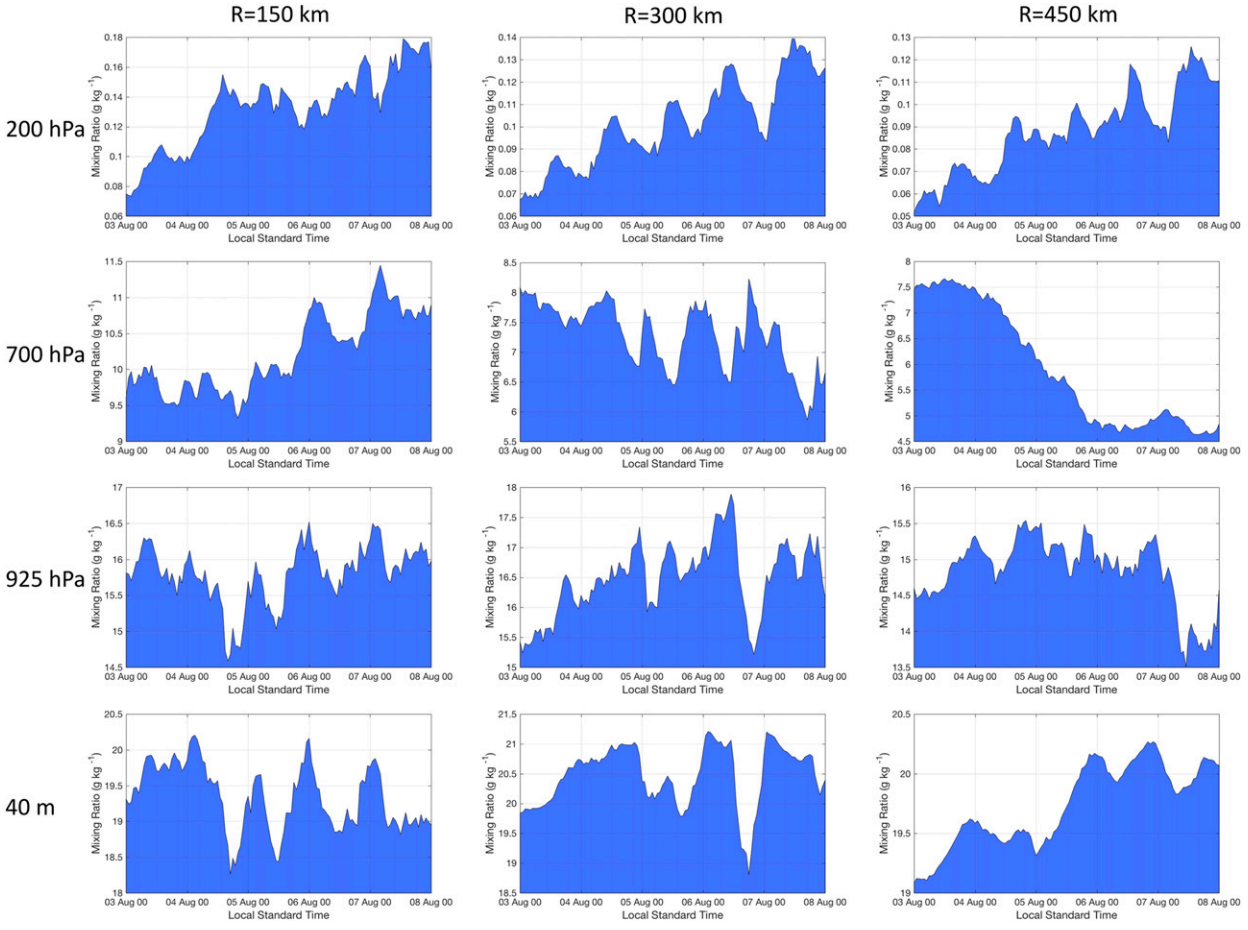

FIG. 11. Azimuthally averaged mixing ratio (g kg^{-1}) derived from the 3–8 Aug HNR1 study period for the 200-hPa, 700-hPa, 925-hPa, and 40-m vertical levels. Analyses include the 150-, 300-, and 450-km radii.

$R \sim$ 200–400 km, and have peak values of ~15–20 m s^{-1}. The 200-hPa radial outflow bursts are also regularly interrupted by outflow minima that peak from the late evening to early morning hours each day and are roughly a factor of 2 weaker (Fig. 15). The positive surges in V_r are coincident in time with the diurnal patterns shown in OLR (Fig. 2), as well as 200-hPa ice mixing ratio, θ, and mixing ratio, highlighting that TC diurnal pulses are associated with marked upper-level signals in both thermodynamics and kinematics. Although there does not appear to be a robust upper-level diurnal signal in radial winds inside of ~150 km, diurnal outflow variability beyond this radius is robust.

In the midlevels of the atmosphere (e.g., 700 hPa), there is a distinct diurnal pattern of enhanced inflow (2–5 m s^{-1}) each day that peaks in the early morning and is concentrated at R = 150–300 km (Fig. 15). These inflow surges occur prior to and radially inward of the 200-hPa outflow bursts that were previously discussed and are interspersed by periods of weak or even near-zero inflow that peak from the late evening to early morning hours each day. Finally, on the inside edge of these inflow bursts ($R \sim$ 25–150 km) there are areas of outflow ranging from 0.5 to 3 m s^{-1}. The diurnal patterns of inflow and outflow suggest that there are favored times of day (approximately midnight to 0600 LST) when local midlevel convergence is maximized and could represent times when the TC is more susceptible to midlevel ventilation (Tang and Emanuel 2012).

At lower levels, diurnal tendencies of V_r are evident from R = 100–450 km (Fig. 15). Peak inflow (~12–18 m s^{-1}) tends to occur in the late evening to early morning hours and is interrupted by periods of relatively weaker inflow (5–12 m s^{-1}) that reach a minimum from the late morning to afternoon hours. These peaks and ebbs in low-level V_r appear to propagate away from the storm each day and the V_r magnitude steadily increases as the simulation progresses and the storm grows and intensifies. The flow patterns suggest that TC inflow and surface fluxes (not shown) are maximized

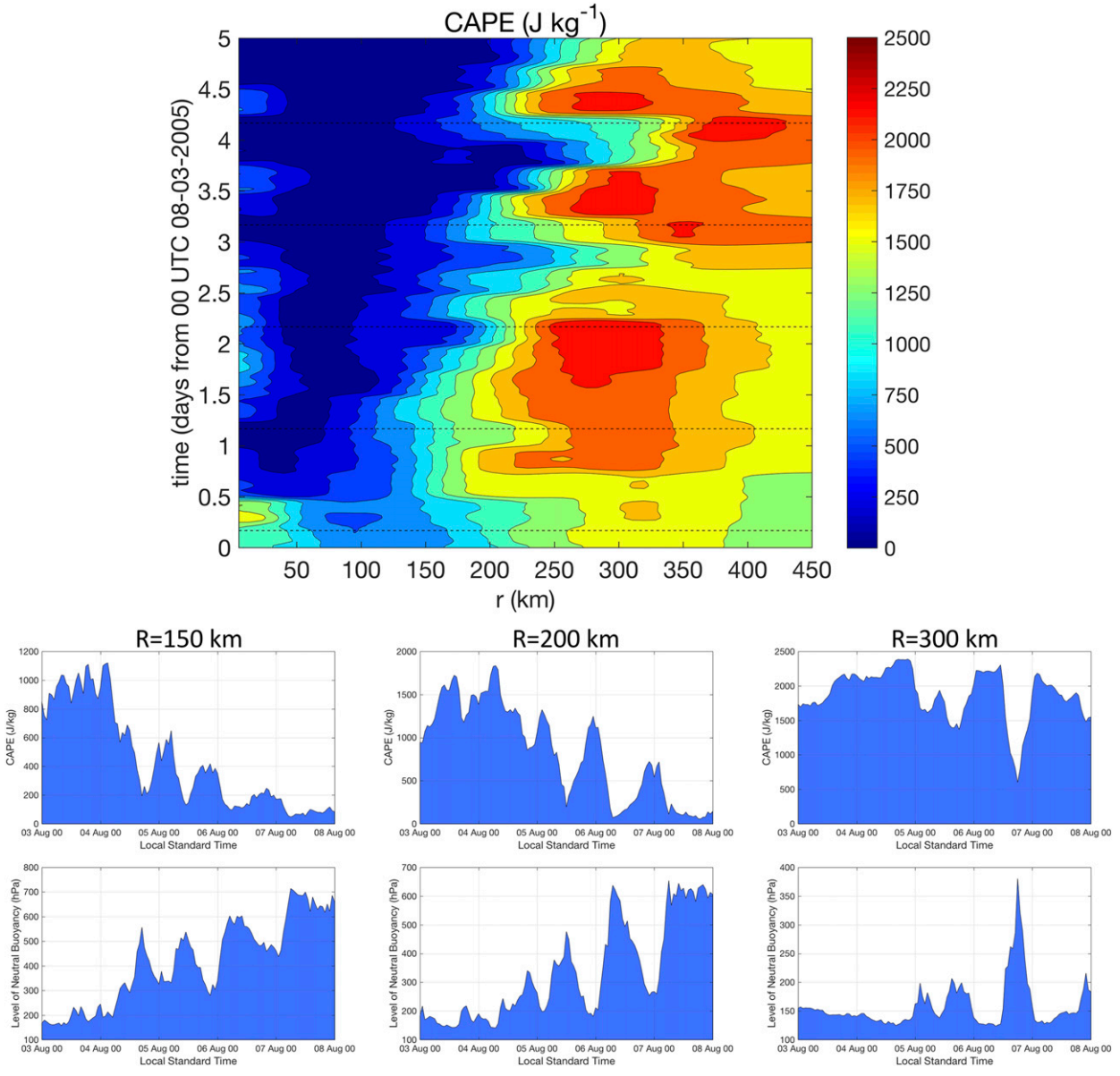

FIG. 12. (top) Hovmöller diagram of azimuthally averaged CAPE (J kg^{-1}) derived from the 3–8 Aug HNR1 study period. Dashed black lines denote 0000 LST during each day of the simulation. Radii are analyzed relative to the TC center and extend out to R = 450 km. (bottom) Azimuthally averaged CAPE and the level of neutral buoyancy (LNB) derived from the 3–8 Aug HNR1study period at the 150-, 200-, and 300-km radii.

just before and after local midnight from R = 100–200 km and peak at larger radii (200+ km) in the early to late morning. It should be noted that diurnal peaks in low-level inflow coincide with peaks in low-level moisture that were discussed in section 3b and shown in Figs. 10 and 11.

The maximum near-surface inflow peaks around and shortly after local midnight, while maximum upper-level outflow peaks around local noon. This ~10–12-h offset in time suggests that the mechanism(s) driving the TCDC does not initiate radial flow simultaneously throughout the depth of the storm.

3) TANGENTIAL WIND (NEAR SURFACE TO UPPER LEVEL)

Tangential winds V_t in the HNR1 TC exhibit marked diurnal signals throughout the troposphere and are most pronounced in the upper levels (e.g., 200 hPa). Figure 16 shows the occurrence of episodic oscillations in upper-level V_t that are particularly apparent from R = 150–450 km.

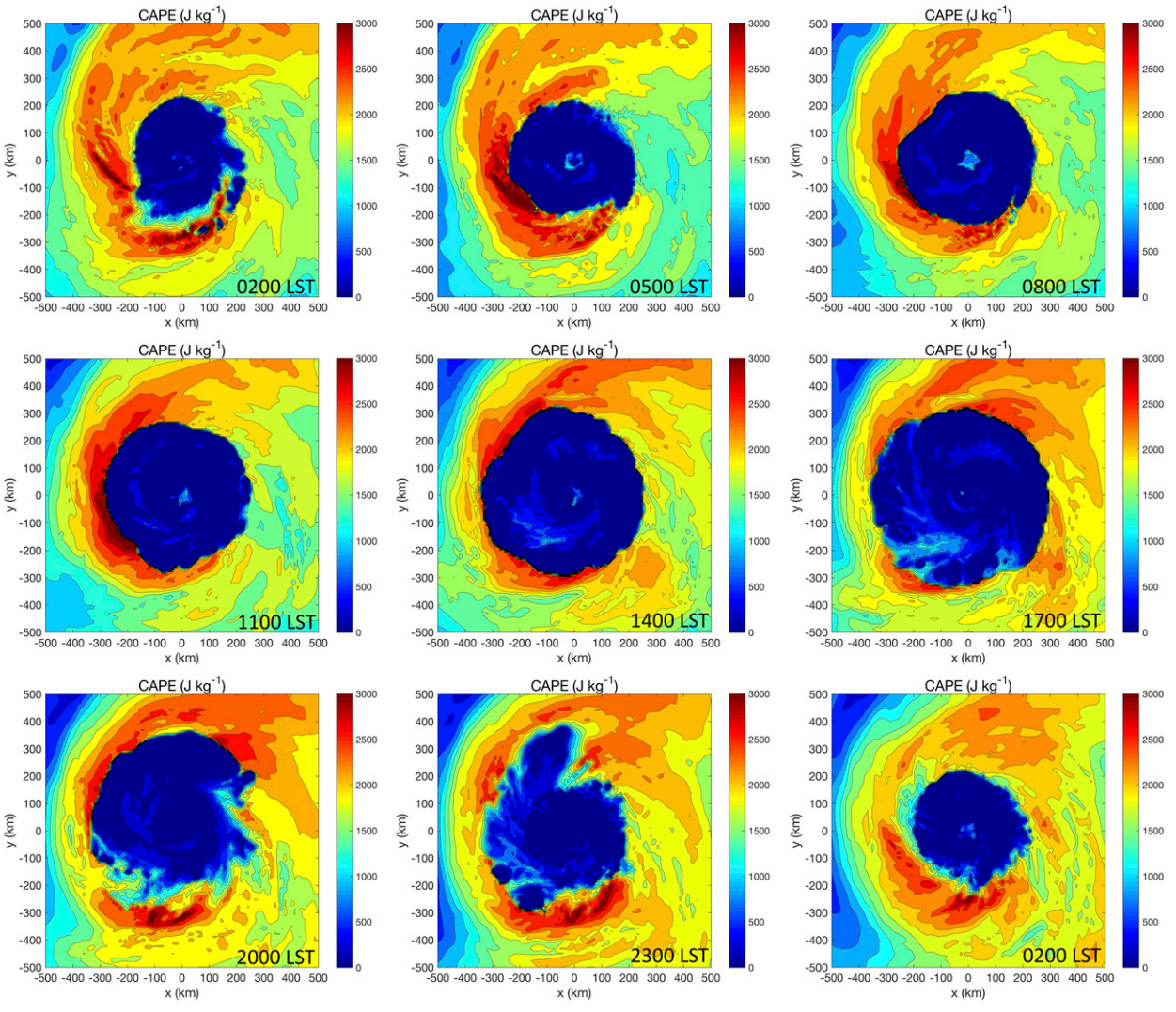

FIG. 13. CAPE (J kg^{-1}) derived from the HNR1 for 6–7 Aug. Images are 3-hourly from (top left) 0200 LST (0600 UTC) 6 Aug to (bottom right) 0200 LST (0600 UTC) 7 Aug.

Peaks in V_t occur in the mid- to late afternoon at R = 300 km and in the late afternoon to early evening at R = 450 km and similar to radial wind, V_t peaks are regularly interrupted by lulls that are a factor of 1.5–5 times weaker at radii ranging from 200 to 450 km.

The midlevels (e.g., 700 hPa) of the HNR1 TC show a relatively more muted V_t diurnal signal that is more pronounced at larger radii (Fig. 16). This figure indicates subtle diurnal oscillations with maxima that occur in the early to midafternoon and minima around local midnight. Lower-level (e.g., 925 hPa and 40 m) diurnal fluctuations in V_t, although not as pronounced as at upper levels, are clearly evident from R = 150–450 km and are particularly robust at R = 300 km (Fig. 16). Here, peak values of V_t tend to occur in the late morning to early afternoon and reach a minimum in the evening, propagating radially at speeds of 5–10 m s^{-1}, which is similar to those described by Dunion et al. (2014). These analyses suggest that there are favored times of day for maximum and minimum values in the magnitude of V_t in the upper, mid-, and lower levels of the HNR1 TC. Amplitudes of these diurnal variations are as high as 10–12, 1–2, and 5–7 m s^{-1}, respectively.

4) VERTICAL WIND

Vertical wind w in the HNR1 TC shows a distinct diurnal pattern that appears to propagate away from the storm each day at speeds similar to previously discussed variables (Fig. 17). At upper levels (e.g., 200 hPa), peaks in w appear at R = 150–200 km in the late morning and

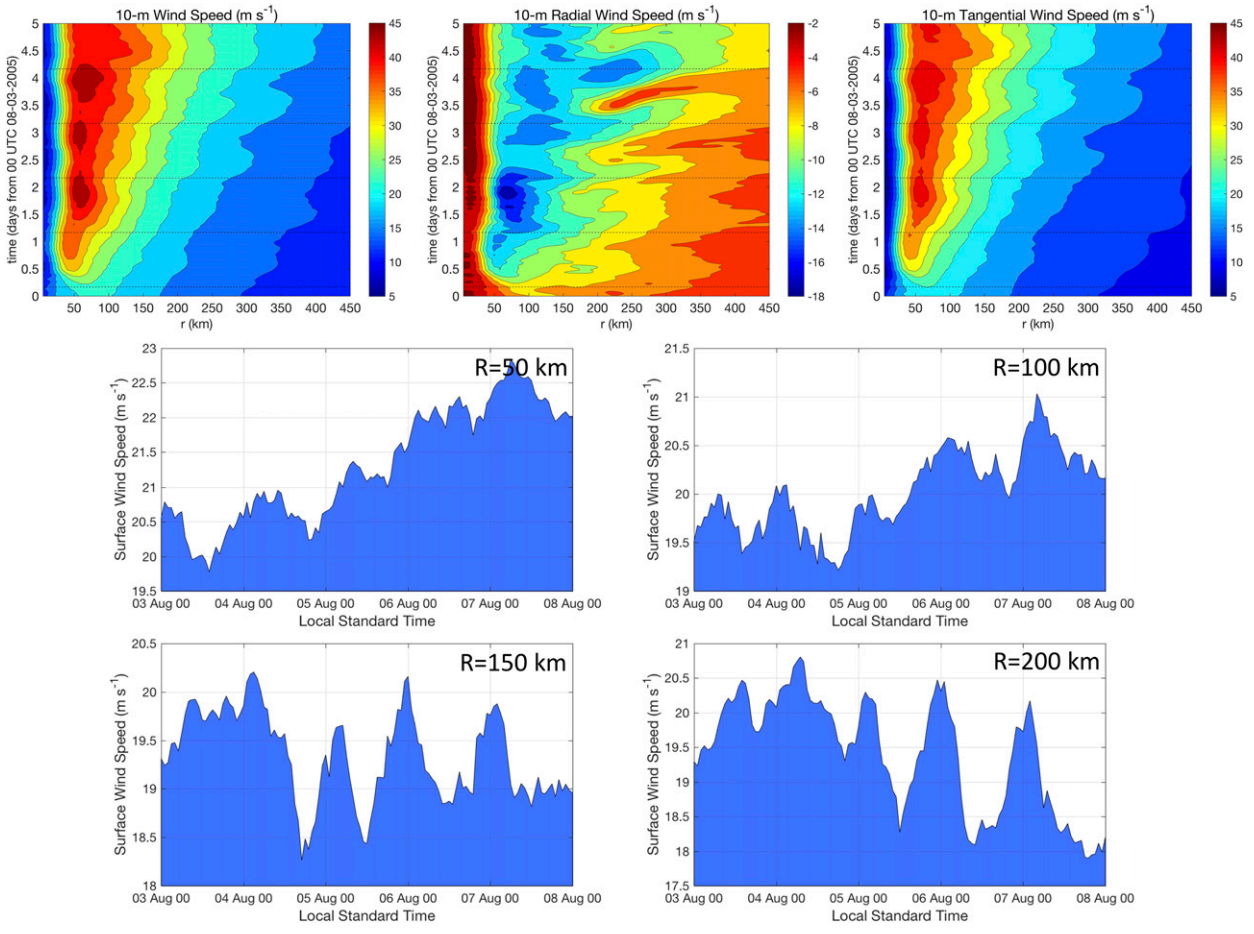

FIG. 14. (top) Hovmöller diagrams of azimuthally averaged 10-m surface winds ($m\,s^{-1}$) derived from the 3–8 Aug HNR1 study period for (left) wind speed, (middle) radial wind speed, and (right) tangential wind speed. Dashed black lines denote 0000 LST during each day of the simulation. Radii are analyzed relative to the TC center and extend out to $R = 450$ km. (bottom) Plots of azimuthally averaged 10-m surface winds ($m\,s^{-1}$) derived from the 3–8 Aug HNR1 study period for 50-, 100-, 150-, and 200-km radii.

propagate to peripheral radii through the early to late afternoon. Maxima in w range from ~0.1 to 0.5 $m\,s^{-1}$, while interspersed minima reach magnitudes close to zero and are occasionally even negative (Fig. 17). Although the upper-level diurnal signal of w is evident at $R \sim 150$–450 km, this figure shows that the magnitudes of the peaks are highest from $R \sim 150$–250 km and generally decrease with increasing radius from the storm.

Diurnal signals of w in the lower to midlevels are less defined than in the upper levels (Fig. 17). However, two-dimensional map analyses of w throughout the study period indicate that w marks the position of the TC diurnal pulses quite clearly and is seen as a narrow (~10–20 km wide) ring of enhanced w that radially propagates away from the storm and has a tropical squall line–like appearance (Fig. 18). The relatively limited radial width of this feature coupled with slight azimuthal asymmetries in the HNR1 TC diurnal pulse signal (i.e., enhanced w) may be somewhat muting the w signal when it is azimuthally averaged (e.g., Fig. 17). Figure 18 shows a 6-hourly progression of a TC diurnal pulse from 0600 UTC (0200 LST) to 1800 UTC (1400 LST) 6 August and shows a semicircular signal in w that is propagating away from the storm each day, reaches $R \sim 300$ km in the afternoon, and is evident through a deep layer of the troposphere from 150 to 925 hPa (not shown). This figure suggests that TC diurnal pulses are associated with distinct peaks in w with updrafts that range from ~1 to 3 $m\,s^{-1}$ and trailing 0.5–2 $m\,s^{-1}$ lower to midlevel downdrafts that appear to be favored behind (radially inward of) the TC diurnal pulse. The couplets of highly symmetric updrafts and downdrafts suggest that TC diurnal pulses may be tropical squall-line features or gravity waves moving/propagating away from the storm each day similar to the outer rainbands that Moon and Nolan (2015) showed to be

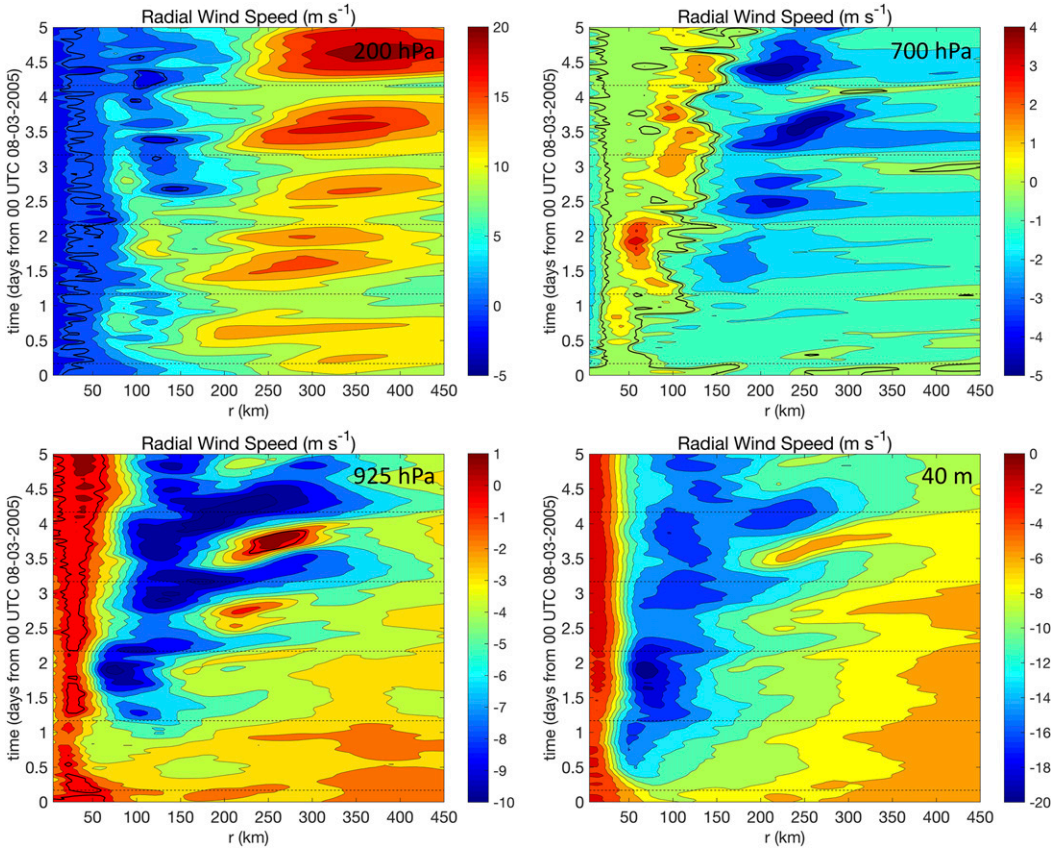

FIG. 15. Hovmöller diagrams of azimuthally averaged radial wind ($m\,s^{-1}$) derived from the 3–8 Aug HNR1 study period for 200 hPa, 700 hPa, 925 hPa, and 40 m. Bold contours indicate regions of zero radial wind and dashed black lines denote 0000 LST during each day of the simulation. Radii are analyzed relative to the TC center and extend out to 450 km.

squall lines with outward-propagating cold pools. The timing of these propagating TC diurnal pulse signals in w also correspond well with the TCDC clock presented by Dunion et al. (2014). Similar analyses made on 4, 5, and 7 August (not shown) indicate a nearly identical TC diurnal pulse signature in w that is also highly symmetric and propagating away from the storm.

d. Precipitation

1) RAIN RATE

Rain rate shows a distinct TCDC pattern and is especially evident from R = 100–300 km (Fig. 19). Similar to analyses of temperature, moisture, and winds, radially propagating signals in rain rate can be seen throughout the study period, but are particularly robust from 5 to 8 August (Fig. 19). Peaks occur in the late evening to early morning hours in the inner core (e.g., R = 100–150 km) and in the early to late morning farther from the storm (e.g., R = 200–250 km, Fig. 19). Conversely, rain-rate minima occur in the late morning to midafternoon at R = 100–150 km and in the late afternoon to late evening at R = 200–250 km.

2) SIMULATED RADAR REFLECTIVITY

Analyses of simulated radar reflectivity show a robust propagating diurnal signal that extends throughout the troposphere (Fig. 20). Diurnal oscillations in this parameter range from ~10 to 30 dBZ and are especially evident from R = 100–300 km. Not surprisingly, these patterns of reflectivity closely resemble those of rain rate and given the diurnal signal of reflectivity, it is plausible that aircraft equipped with radar (e.g., C-band or X-band Doppler) could be used to track the evolution of the TCDC. Additionally, given the common practice of empirically estimating rainfall from land-based radar, the TCDC could be an important consideration regarding the analysis of quantitative precipitation forecasts for landfalling TCs.

3) CONDENSATE

Figure 21 shows HNR1 TC radius–height plots of azimuthally averaged total condensate (hereafter, q_{total})

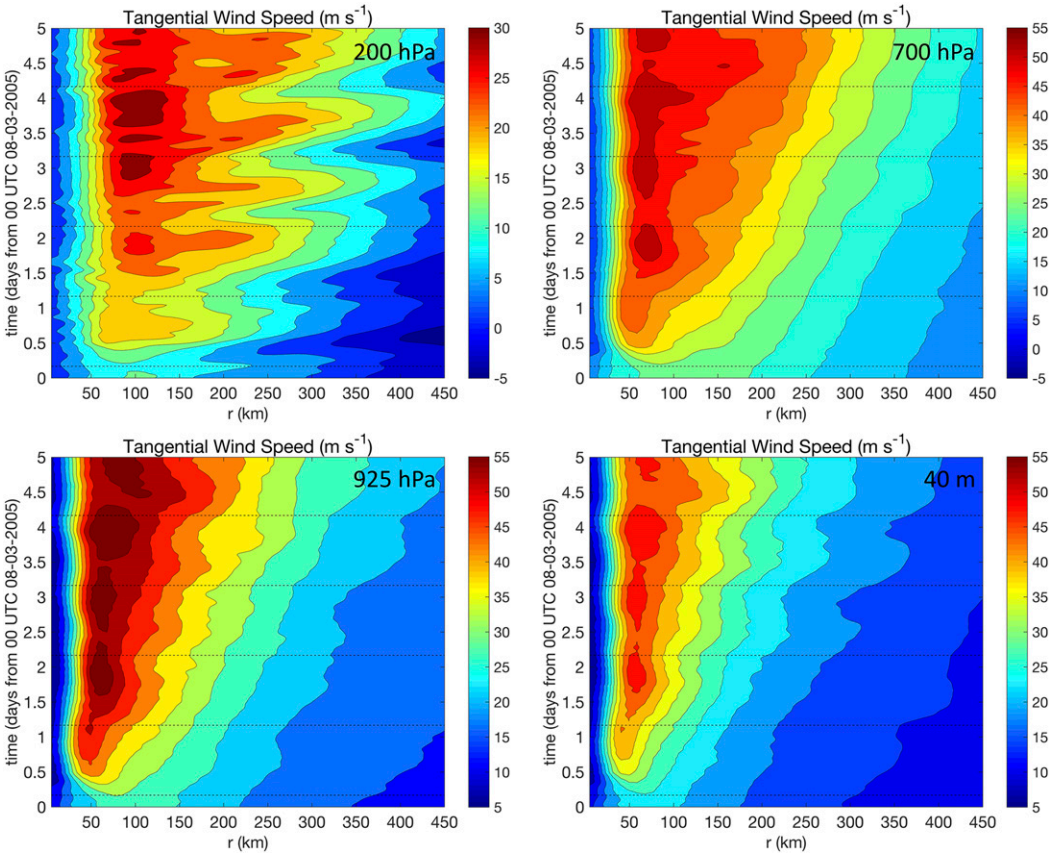

FIG. 16. Hovmöller diagrams of azimuthally averaged tangential wind (m s^{-1}) derived from the 3–8 Aug HNR1 study period for 200 hPa, 700 hPa, 925 hPa, and 40 m. Dashed black lines denote 0000 LST during each day of the simulation. Radii are analyzed relative to the TC center and extend out to $R = 450$ km.

and vertical wind during the most pronounced day of diurnal fluctuations in simulated radar reflectivity (6 August). This figure suggests that an area of enhanced moisture and vertical winds forms outside the eyewall ($R \sim 75$–150 km) around local midnight that day. The feature appears to be elevated above the surface, has a vertical extent of ~2–14 km, and clearly propagates away from the storm throughout the day, reaching radii of approximately 200, 250, and 300 km at 0600, 1200, and 1800 LST respectively. This region of enhanced moisture and vertical winds may, in fact, be linked to a TC diurnal pulse that is propagating away from the storm, and in the afternoon, it becomes coupled with a trailing downdraft and area of suppressed low-level moisture. The area of suppressed q_{total} behind the TC diurnal pulse is prominent at 1200 LST and especially 1800 LST, extends from the surface to ~4 km, and is the signature of a cold pool. In fact, the entire propagating feature (TC diurnal pulse and cold pool) looks remarkably similar to a tropical squall line (Gamache and Houze 1982). If TC diurnal pulses do indeed behave like tropical squall-line features that propagate away from the storm each day, some kind of common lifting mechanism, such as a gravity wave, frontal feature, or outflow boundary is suggested. Also, since tropical squall lines develop in regions of optimal moisture, stability, and lift, it is possible that the priming of the environment just outside the inner core ($R \sim 150$–350 km) during the nighttime that was discussed in section 3b(3) (i.e., elevated LNB and enhanced CAPE) could support the existence of a convectively active, long-lived (several hours) tropical squall-line feature. Tropical squall lines are also partly sustained via the production of lift via outflow boundaries. Dunion et al. (2014) noted that arc clouds (i.e., outflow boundaries) often appear to form along the leading edges of TC diurnal pulses, which further supports this idea that TC diurnal pulses associated with the TCDC behave like tropical squall lines. Whatever this feature is, it repeats over multiple days of the HNR1 study period and appears to have origins in a deep, yet elevated layer at radii where radiation tendencies support reduced static

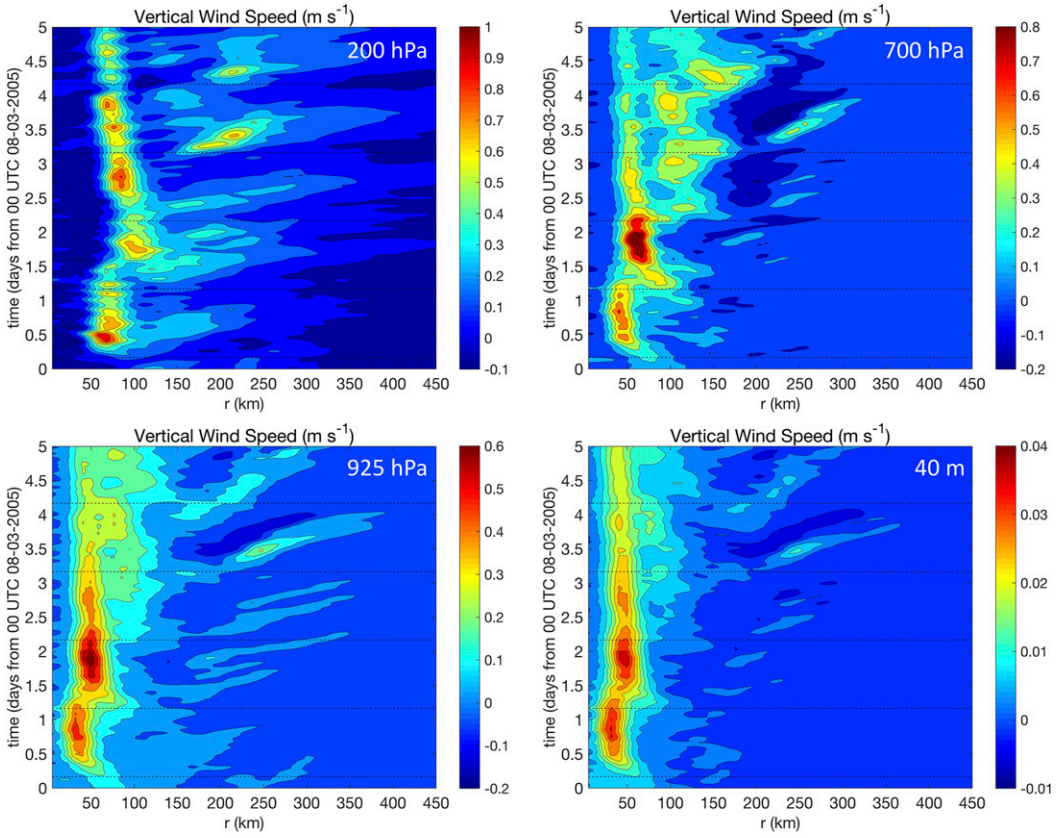

FIG. 17. Hovmöller diagrams of azimuthally averaged vertical wind ($m\,s^{-1}$) derived from the 3–8 Aug HNR1 study period for 200 hPa, 700 hPa, 925 hPa, and 40 m. Dashed black lines denote 0000 LST during each day of the simulation. Radii are analyzed relative to the TC center and extend out to 450 km.

stability and enhanced upper-level outflow release near and after sunset each day. The TCDC conceptual clock presented by Dunion et al. (2014) also suggests that as this feature propagates away from the storm, it is located at R ~ 200–300 km during the early to late morning. Analyses of the LNB [section 3b(3), Fig. 12] indicate that the propagation of this feature coincides with diurnal minima in LNB heights ($z \sim 500$–600 hPa) in this region of the peripheral TC environment, which could act to limit its vertical extent as it moves away from the storm. Although the exact mechanism causing the diurnal features described above is not clear, their regular occurrence does suggest that radiation tendencies that are being driven by the solar cycle are a key controlling factor.

4. Discussion and conclusions

The goal of this study was to examine a high-resolution, high-quality simulation of a hurricane to look for signals of the TC diurnal cycle (TCDC) in the model, characterize these signals in time and space, and better understand the processes that cause them. Through this work we have highlighted a marked radially propagating diurnal signal in the hurricane nature run of N13 that becomes robust when the storm reaches category 2 intensity (i.e., $\geq 43\,m\,s^{-1}$), is embedded in a low vertical wind shear environment (i.e., $\leq 7.5\,m\,s^{-1}$), and is sufficiently removed from land (i.e., ≥ 300 km). When these thresholds described by Dunion et al. (2014) are satisfied, various diurnal signals in radiation tendency, thermodynamics, static stability, winds, and precipitation become apparent in the TC inner core and surrounding environment. Details of these signals are discussed in the context of both time and space and may be applicable to other simulated TCs where the employed model includes a solar cycle and the simulated storm satisfies the aforementioned conditions.

It is hypothesized that enhanced nighttime radiational cooling that is greatest in the TC outflow layer (relative to surrounding cloud-free air) may act to destabilize and prime, or precondition, the TC environment for triggering of the TCDC via one of the mechanisms described by Dunion et al. (2014) (e.g., convectively driven

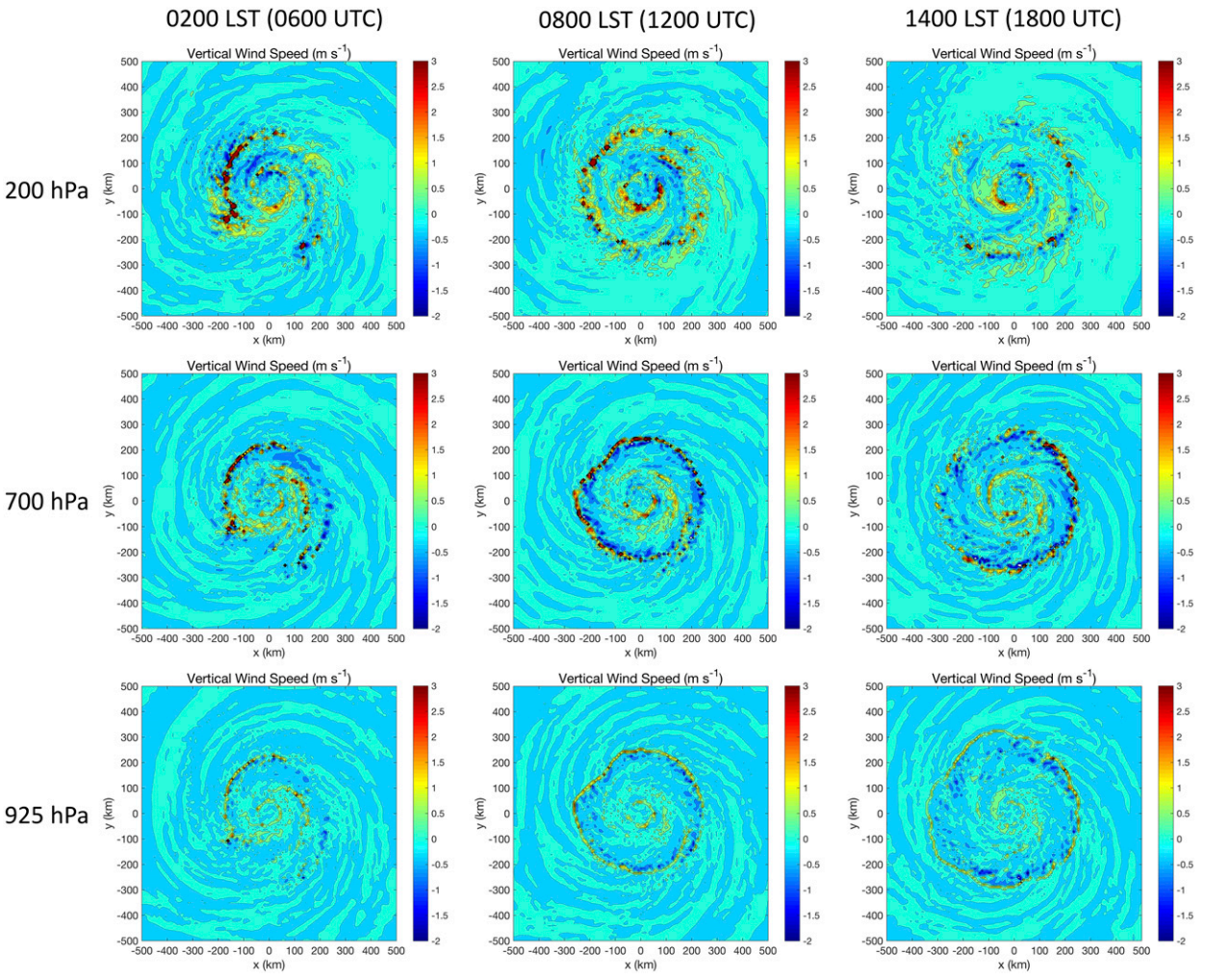

FIG. 18. Plots of vertical wind (m s^{-1}) derived from the HNR1 from 0200–1400 LST (0600–1800 UTC) 6 Aug at 200, 700, and 925 hPa. A relatively deep layer semicircular feature is indicated 200–300 km outside of the eyewall that has 1–3 m s^{-1} vertical motion and is propagating away from the TC.

gravity waves, radiatively reduced outflow resistance, cloud vs cloud-free differential heating, seeder–feeder mechanism, or some combination of these mechanisms). During the daytime, the stabilizing effects of shortwave warming suppress TCDC processes in the storm environment, which leads to the culmination of the TCDC each day. If the TCDC and associated TC diurnal pulses are indeed found to be linked to gravity wave features, as suggested by Dunion et al. (2014) and O'Neill et al. (2017), the latter term may be better described as a TC diurnal wave and will be the topic of future work. Figure 22 presents a TCDC-centric schematic summarizing the daytime evolution of TC diurnal pulses, seen as a surge in upper-level outflow that is underlain by radially propagating tropical squall-line-like features with associated gust fronts (i.e., arc clouds), highlights relative minima and maxima of radial outflow and inflow during different times of day, and indicates enhanced vertical winds at the location of the tropical squall line. As the TC diurnal pulse propagates away from the storm during the day, the low to midlevel tropical squall-line feature becomes increasingly shallow with increasing radius from the storm. Key findings from the HNR1 TC analyses reveal the following:

1) *OLR and upper-level ice mixing ratio*: OLR analyses show a distinct diurnal oscillation that appears to propagate away (~5–10 m s^{-1}) from the storm each day beginning at $R \sim 150$ km and eventually reaching $R \sim 450$ km. Peak OLR cooling occurs from ~0600 to 1800 LST and has similar timing to TC diurnal pulses previously described by Dunion et al. (2014). Complimentary analyses of ice mixing ratio at ~200 hPa suggest that a distinct radially propagating

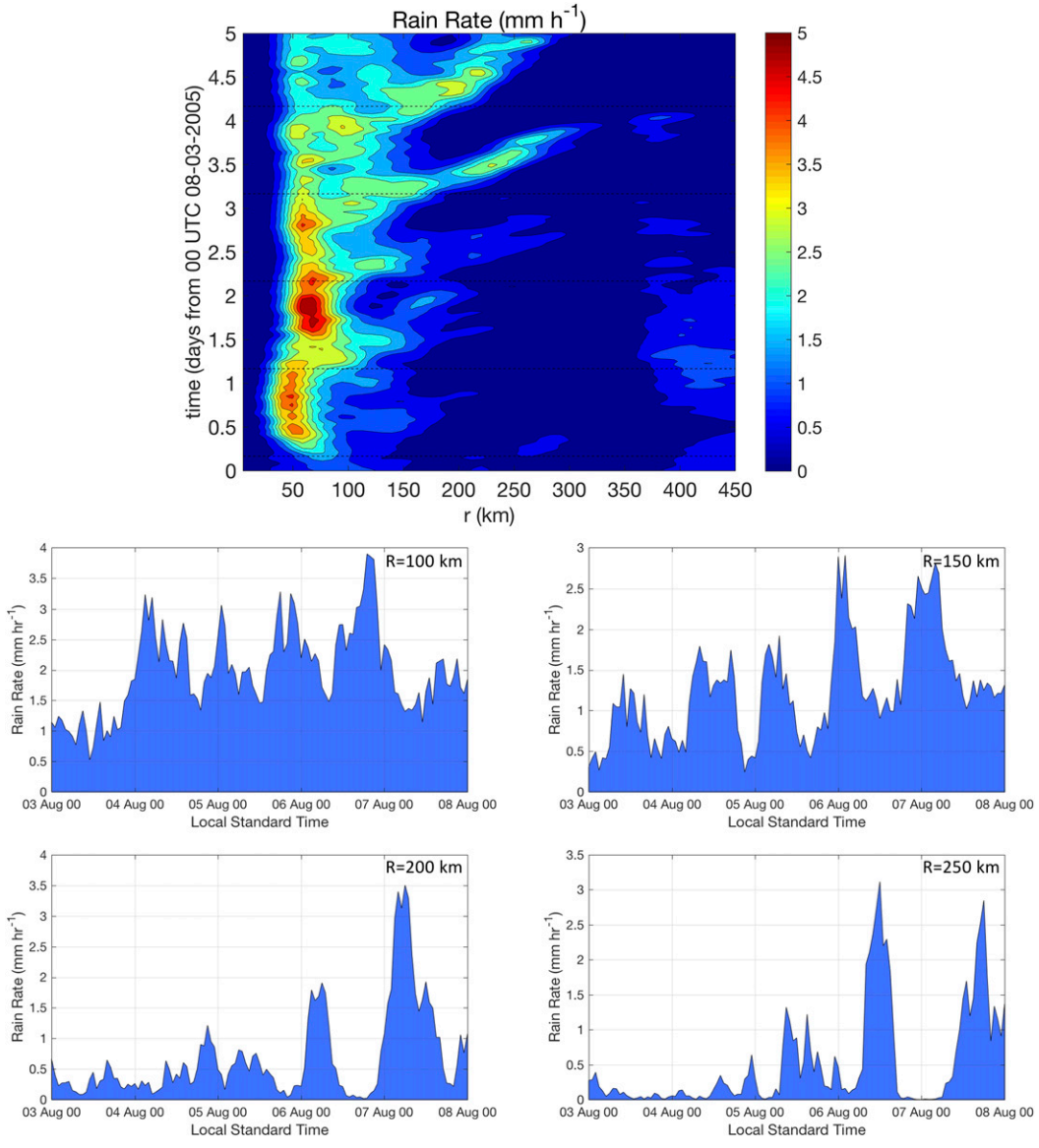

FIG. 19. (top) Hovmöller diagram of rain rate (mm h^{-1}) derived from the 3–8 Aug HNR1 study period. Dashed black lines denote 0000 LST during each day of the simulation. Radius is analyzed relative to the TC center and extends out to $R = 450$ km. (bottom) Plots of azimuthally averaged rain rate (mm h^{-1}) derived from the 3–8 Aug HNR1 study period at the 100-, 150-, 200-, and 250-km radii.

diurnal signal is present in the upper-level outflow layer of the storm.

2) *Thermodynamics*: potential temperature reveals a TCDC signal (especially at radii of ≥150 km) that involves a relatively deep layer of the storm and its surrounding environment. Water vapor mixing ratio indicates a propagating diurnal signal that is particularly pronounced near the TC outflow layer and at lower levels (~925 hPa to the near surface). Diurnal oscillations in low-level moisture appear to manifest as periodic minima that are concentrated at $R \sim 100$–300 km, extend from the surface up to $z \sim 4$ km, and may be linked to large arc cloud features that form along the leading edge of TC diurnal pulses. This suggests that TC diurnal pulses may behave like tropical squall-line features with associated outflow boundaries that propagate away from the HNR1 storm each day.

3) *Radiation, LNB, and CAPE:* diurnal fluctuations of mid- to upper-level ($z \sim 4$–12 km) shortwave and longwave radiation in the TC inner core and surrounding environment appear to have profound

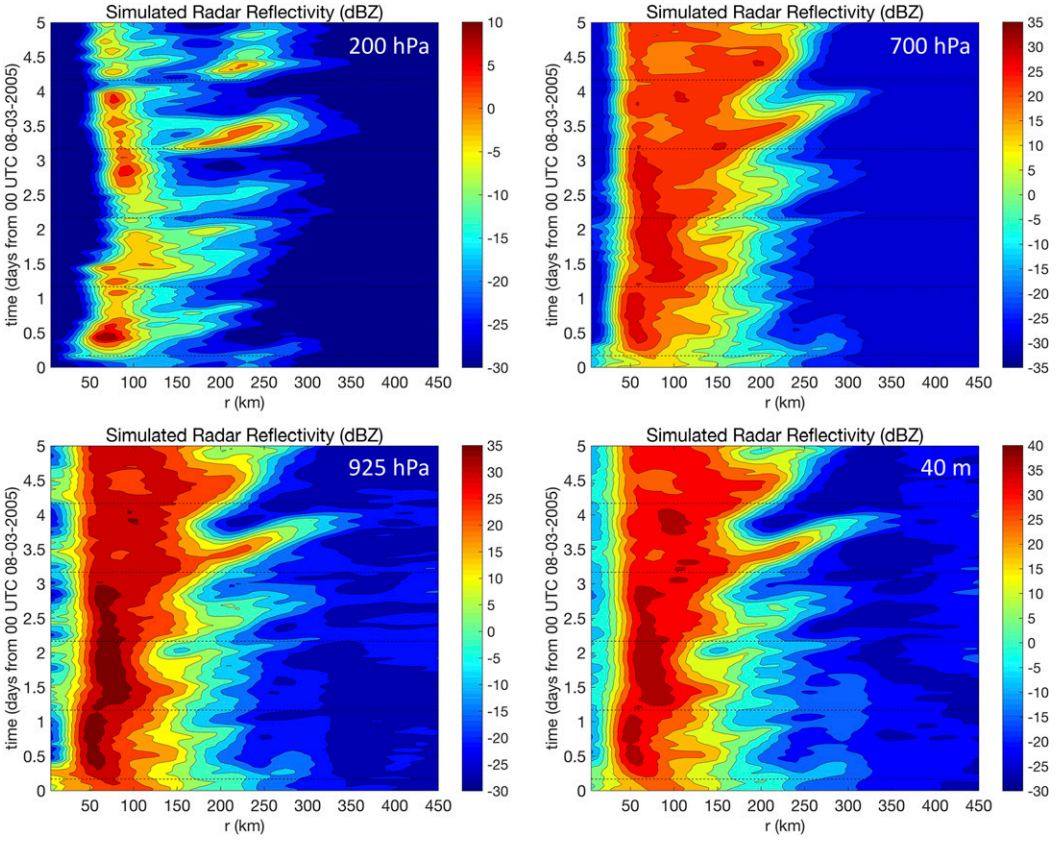

FIG. 20. Hovmöller diagrams of simulated radar reflectivity (dBZ) derived from the 3–8 Aug HNR1 study period for 200 hPa, 700 hPa, 925 hPa, and 40 m. Dashed black lines denote 0000 LST during each day of the simulation. Radii are analyzed relative to the TC center and extend out to $R = 450$ km.

effects on the level of neutral buoyancy (LNB) and CAPE in the storm environment each day. Although the presence of the TC warm core and radiation tendencies consistently support very low CAPE (~0–500 J kg^{-1}) inside the TC inner core ($R \sim \leq 150$ km), the region just outside the inner core ($R \sim 150$–350 km) experiences marked diurnal fluctuations of the LNB and CAPE. Here, these parameters fluctuate by as much as 450 hPa and 1500 J kg^{-1}, respectively, and promote a convectively favorable environment in the late evening to early morning hours. This nighttime enhancement of CAPE at $R \sim 150$–350 km could favor convectively active TC diurnal pulses and could partly explain why they are seen to form at $R \sim 150$ km after sunset each day in both satellite imagery and the HNR1.

4) *10-m surface winds*: 10-m surface winds show a clear diurnal signal and indicate that there are marked alternating periods of enhanced (evening to early morning hours) and suppressed (midmorning to afternoon hours) surface winds and low-level inflow each day, particularly along the periphery and just outside the storm's inner core ($R \sim 100$–350 km). These findings suggest that the TCDC has implications for forecasting TC intensity and structure and will be investigated in future work.
5) *Radial winds*: Radial winds in the HNR1 TC show significant diurnal oscillations near the level of the outflow layer with regular outward bursts that begin near $R \sim 150$ km in the morning hours each day and steadily propagate out to peripheral radii (e.g., $R \sim$ 350–450 km) during the afternoon. These outflow maxima are interrupted by lulls in outflow that peak in the late evening and are a factor of 2 weaker than the periods of maximum outflow. Midlevel (e.g., 700 hPa) radial wind also has a diurnal inflow peak in the midmorning and could be a time when the TC is more susceptible to midlevel ventilation. Low-level (~925 hPa to the surface) radial winds in the HNR1 TC also indicated that peak inflow at $R \sim 100$–200 km occurs in the early morning hours and is interspersed by periods of relatively weaker inflow that are weakest in the late morning to afternoon.
6) *Vertical winds*: clear diurnal signals in vertical wind occur near the level of the TC outflow layer

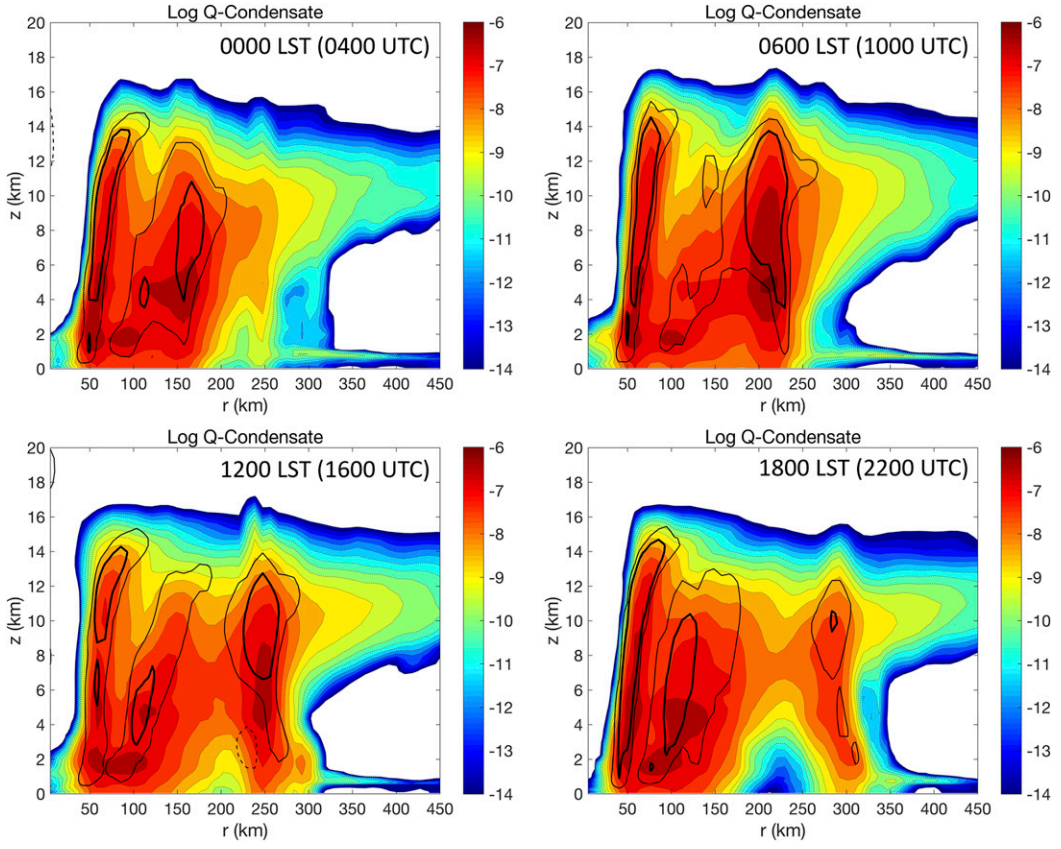

FIG. 21. The 6-hourly radius–height plots of Q condensate (q_{total}) from the HNR1 TC at 0000–1800 LST (0400–2200 UTC) 6 Aug. Dashed black, solid black, and thick solid black contours indicate azimuthal mean vertical winds of -0.25, $+0.25$, and $+0.5\,\text{m s}^{-1}$, respectively.

(~200 hPa), but are less defined in the lower (e.g., 925 hPa to the near surface) and especially midlevels (e.g., 700 hPa). Two-dimensional plots of vertical wind made during several of the days of HNR1 TC peak intensity reveal narrow (~10–20 km wide), highly symmetric rings of enhanced vertical winds that are coupled with convection and propagate away from the storm each day. These features appear to involve a deep layer of the troposphere and their propagation closely matches the TCDC conceptual clock presented by Dunion et al. (2014). They are also similar in appearance to the 37- and 85-GHz microwave convective rings that were described in that work and may be a signature of the TC diurnal pulse.

7) *Precipitation*: rain rates and simulated radar reflectivity show a strong outwardly propagating diurnal signal. Maxima (minima) in precipitation peak in the late evening to early morning (late morning to midafternoon) in the inner core and in the early to late morning (late afternoon to late evening) farther from the storm (e.g., R = 200–450 km). These trends suggest that the TCDC may have implications for quantitative precipitation forecasting and TC structure. Analyses of q_{total} and vertical wind suggested that TC diurnal pulses might at least partially behave like tropical squall lines that are accompanied by outflow boundaries (i.e., arc clouds).

The hurricane nature run reveals robust diurnal signals in radiation, thermodynamics, static stability, winds, and precipitation. Since the HNR1 was produced using the WRF Model, the TCDC signals highlighted here have implications on a wide range of research studies that have utilized this model, as well as NOAA's operational HWRF Model. Identifying TCDC signals in models like WRF and HWRF offers opportunities to both further our understanding of TCDC processes and to understand how the TCDC affects the representation, analyses, and forecasts of TCs in numerical simulations. Future work will continue to integrate satellite data, numerical model simulations, and observations of the TCDC with a goal of continued advancement of our understanding of this possibly fundamental TC process.

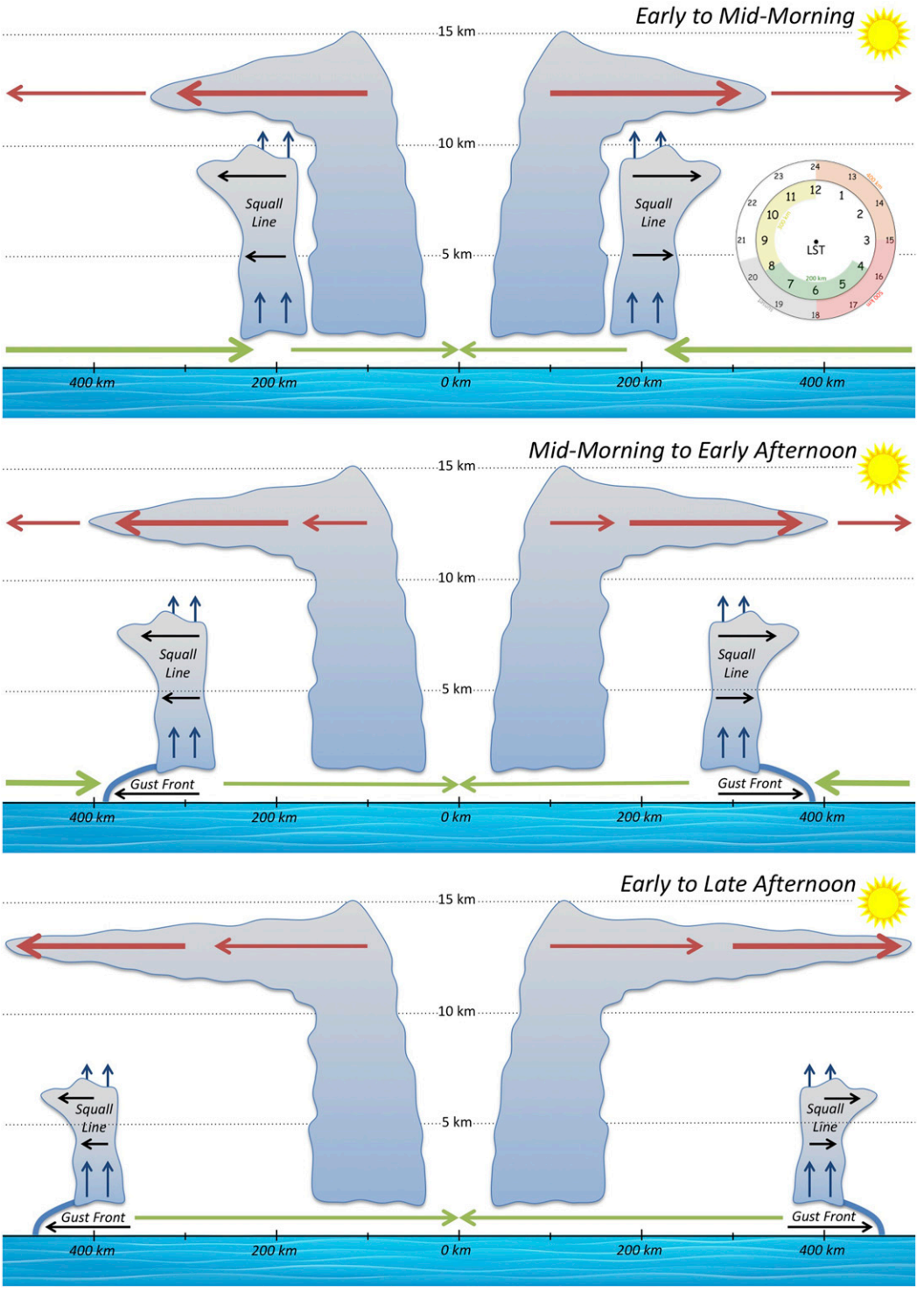

FIG. 22. Schematic showing the evolution of a radially propagating TC diurnal pulse from the early morning to late afternoon. Upper- level radial outflow (red arrows), lower-level radial inflow (green arrows), and enhanced vertical wind at the location of the TC diurnal pulse (i.e., tropical squall line, blue arrows) are shown. Gust fronts favored to form along the leading edge of the tropical squall line beginning in the midmorning to late afternoon when it is located at $R \sim 300$–400 km are shown. Thickness of the radial outflow and inflow lines indicate relative strength at different times of day relative to the position of the tropical squall line. The depth of the tropical squall line is also suggested to lessen as it propagates away from the storm due to a lowering LNB that reaches a minimum in the afternoon. The TC diurnal clock presented by Dunion et al. (2014) is included for reference.

Acknowledgments. The authors thank John Molinari, Ryan Torn, Lance Bosart, Frank Marks, and Chris Velden (a.k.a. the "hive") for their many insightful discussions related to the TC diurnal cycle and this work. This paper benefited from reviews by Jonathan Zawislak and Gus Alaka from the University of Miami/CIMAS–NOAA/AOML/HRD, James Ruppert from the Max Planck Institute for Meteorology, and John Knaff from NOAA/NESDIS. This research is supported by NASA Grant NNX10AU44G from the Hurricane and Severe Storm Sentinel (HS3) Project, Office of Naval Research Program Element (PE) 0601153N Grant N000141410132, and by NOAA Grant NA14OAR4830172 from the Unmanned Aircraft Systems (UAS) Program. D. Nolan was supported in part by Grant NNX14AB19G from the NASA *CloudSat/CALIPSO* Science Team program.

REFERENCES

Andersson, E., and M. Masutani, 2010: Collaboration on observing system simulation experiments (Joint OSSE). *ECMWF Newsletter*, No. 123, ECMWF, Reading, United Kingdom, 14–16, http://www.emc.ncep.noaa.gov/research/JointOSSEs/publications/JOSSE-Publication-files/Andersson_JOSSE_ECMWF_News_No123.pdf.

Atlas, R., and Coauthors, 2015: Observing system simulation experiments (OSSEs) to evaluate the potential impact of an optical autocovariance wind lidar (OAWL) on numerical weather prediction. *J. Atmos. Oceanic Technol.*, **32**, 1593–1613, https://doi.org/10.1175/JTECH-D-15-0038.1.

Browner, S. P., W. L. Woodley, and C. G. Griffith, 1977: Diurnal oscillation of cloudiness associated with tropical storms. *Mon. Wea. Rev.*, **105**, 856–864, https://doi.org/10.1175/1520-0493(1977)105<0856:DOOTAO>2.0.CO;2.

Bu, Y. P., R. G. Fovell, and K. L. Corbosiero, 2014: Influence of cloud–radiative forcing on tropical cyclone structure. *J. Atmos. Sci.*, **71**, 1644–1662, https://doi.org/10.1175/JAS-D-13-0265.1.

Demuth, J., M. DeMaria, and J. A. Knaff, 2006: Improvement of advanced microwave sounder unit tropical cyclone intensity and size estimation algorithms. *J. Appl. Meteor. Climatol.*, **45**, 1573–1581, https://doi.org/10.1175/JAM2429.1.

Donelan, M. A., B. K. Haus, N. Reul, W. J. Plant, M. Stiassnie, H. C. Graber, O. B. Brown, and E. S. Saltzman, 2004: On the limiting aerodynamic roughness of the ocean in very strong winds. *Geophys. Res. Lett.*, **31**, 4539–4542, https://doi.org/10.1029/2004GL019460.

Dunion, J. P., 2011: Rewriting the climatology of the tropical North Atlantic and Caribbean Sea atmosphere. *J. Climate*, **24**, 893–908, https://doi.org/10.1175/2010JCLI3496.1.

——, C. D. Thorncroft, and C. S. Velden, 2014: The tropical cyclone diurnal cycle of mature hurricanes. *Mon. Wea. Rev.*, **142**, 3900–3919, https://doi.org/10.1175/MWR-D-13-00191.1.

Dunn, G. E., and B. I. Miller, 1960: *Atlantic Hurricanes.* Louisiana State University Press, 377 pp.

Gallina, G. M., and C. S. Velden, 2000: A quantitative look at the relationship between environmental vertical wind shear and tropical cyclone intensity change utilizing enhanced satellite derived wind information. Preprints, *24th Conf. on Hurricanes and Tropical Meteorology*, Ft. Lauderdale, FL, Amer. Meteor. Soc., 7A.4, https://ams.confex.com/ams/last2000/webprogram/Paper12361.html.

Gamache, J. F., and R. A. Houze Jr., 1982: Mesoscale air motions associated with a tropical squall line. *Mon. Wea. Rev.*, **110**, 118–135, https://doi.org/10.1175/1520-0493(1982)110<0118:MAMAWA>2.0.CO;2.

Gray, W. M., and R. W. Jacobson, 1977: Diurnal variation of deep cumulus convection. *Mon. Wea. Rev.*, **105**, 1171–1188, https://doi.org/10.1175/1520-0493(1977)105<1171:DVODCC>2.0.CO;2.

Kepert, J. D., and D. S. Nolan, 2014: Reply to "Comments on 'How does the boundary layer contribute to eyewall replacement cycles in axisymmetric tropical cyclones?'". *J. Atmos. Sci.*, **71**, 4692–4704, https://doi.org/10.1175/JAS-D-14-0014.1.

Kossin, J. P., 2002: Daily hurricane variability inferred from GOES infrared imagery. *Mon. Wea. Rev.*, **130**, 2260–2270, https://doi.org/10.1175/1520-0493(2002)130<2260:DHVIFG>2.0.CO;2.

Liu, C., and M. W. Moncrieff, 1998: A numerical study of the diurnal cycle of tropical oceanic convection. *J. Atmos. Sci.*, **55**, 2329–2344, https://doi.org/10.1175/1520-0469(1998)055<2329:ANSOTD>2.0.CO;2.

Mapes, B. E., and R. A. Houze Jr., 1993: Cloud clusters and superclusters over the oceanic warm pool. *Mon. Wea. Rev.*, **121**, 1398–1415, https://doi.org/10.1175/1520-0493(1993)121<1398:CCASOT>2.0.CO;2.

McNoldy, B., B. Annane, S. Majumdar, J. Delgado, L. Bucci, and R. Atlas, 2017: Impact of assimilating CYGNSS data on tropical cyclone analyses and forecasts in a regional OSSE framework. *Mar. Technol. Soc. J.*, **51**, 7–15, https://doi.org/10.4031/MTSJ.51.1.1.

Miyamoto, Y., and T. Takemi, 2015: A triggering mechanism for rapid intensification of tropical cyclones. *J. Atmos. Sci.*, **72**, 2666–2681, https://doi.org/10.1175/JAS-D-14-0193.1.

Moon, Y., and D. S. Nolan, 2015: Spiral rainbands in a numerical simulation of Hurricane Bill (2009). Part II: Propagation of inner rainbands. *J. Atmos. Sci.*, **72**, 191–215, https://doi.org/10.1175/JAS-D-14-0056.1.

Muramatsu, T., 1983: Diurnal variations of satellite-measured TBB areal distribution and eye diameter of mature typhoons. *J. Meteor. Soc. Japan*, **61**, 77–90, https://doi.org/10.2151/jmsj1965.61.1_77.

Navarro, E. L., and G. J. Hakim, 2016: Idealized numerical modeling of the diurnal cycle of tropical cyclones. *J. Atmos. Sci.*, **73**, 4189–4201, https://doi.org/10.1175/JAS-D-15-0349.1.

Nolan, D. S., R. M. Atlas, K. T. Bhatia, and L. R. Bucci, 2013: Development and validation of a hurricane nature run using the joint OSSE nature run and WRF model. *J. Adv. Model. Earth Syst.*, **5**, 382–405, https://doi.org/10.1002/jame.20031.

O'Neill, M. E., D. Perez-Betancourt, and A. A. Wing, 2017: Accessible environments for diurnal-period waves in simulated tropical cyclones. *J. Atmos. Sci.*, **74**, 2489–2502, https://doi.org/10.1175/JAS-D-16-0294.1.

Pollard, R. T., P. B. Rhines, and R. O. R. Y. Thompson, 1972: The deepening of the wind-mixed layer. *Geophys. Fluid Dyn.*, **4**, 381–404, https://doi.org/10.1080/03091927208236105.

Randall, D. A., Harshvardhan, and D. A. Dazlich, 1991: Diurnal variability of the hydrologic cycle in a general circulation model. *J. Atmos. Sci.*, **48**, 40–62, https://doi.org/10.1175/1520-0469(1991)048<0040:DVOTHC>2.0.CO;2.

Rogers, R. F., S. Lorsolo, P. Reasor, J. Gamache, and F. Marks, 2012: Multiscale analysis of tropical cyclone kinematic structure from

airborne Doppler radar composites. *Mon. Wea. Rev.*, **140**, 77–99, https://doi.org/10.1175/MWR-D-10-05075.1.

Ruppert, J. H., and C. Hohenegger, 2018: Diurnal circulation adjustment and organized deep convection. *J. Climate*, **31**, 4899–4916, https://doi.org/10.1175/JCLI-D-17-0693.1.

Tang, B., and K. Emanuel, 2012: A ventilation index for tropical cyclones. *Bull. Amer. Meteor. Soc.*, **93**, 1901–1912, https://doi.org/10.1175/BAMS-D-11-00165.1.

Tang, X., and F. Zhang, 2016: Impacts of the diurnal radiation cycle on the formation, intensity, and structure of Hurricane Edouard (2014). *J. Atmos. Sci.*, **73**, 2871–2892, https://doi.org/10.1175/JAS-D-15-0283.1.

Weickmann, H. K., A. B. Long, and L. R. Hoxit, 1977: Some examples of rapidly growing oceanic cumulonimbus clouds. *Mon. Wea. Rev.*, **105**, 469–476, https://doi.org/10.1175/1520-0493(1977)105<0469:SEORGO>2.0.CO;2.

Xu, K.-M., and D. A. Randall, 1995: Impact of interactive radiative transfer on the macroscopic behavior of cumulus ensembles. Part II: Mechanisms for cloud–radiation interactions. *J. Atmos. Sci.*, **52**, 800–817, https://doi.org/10.1175/1520-0469(1995)052<0800:IOIRTO>2.0.CO;2.

Yang, G., and J. Slingo, 2001: The diurnal cycle in the tropics. *Mon. Wea. Rev.*, **129**, 784–801, https://doi.org/10.1175/1520-0493(2001)129<0784:TDCITT>2.0.CO;2.